

This is a non peer reviewed preprint submitted to EarthArxiv.

DiadFit: An Open-Source Python3 Tool for Peak fitting of Raman Data from silicate melts and CO₂ fluids

Penny E. Wieser¹ and Charlotte DeVitre¹

Earth and Planetary Sciences, UC Berkeley

It was submitted to Volcanica on Oct 25, 2023

We welcome any feedback – it might not work straight out the box for every Raman set up on the planet, but if you send us some spectra, we will tweak it to ensure its useful for your lab!

Any questions – contact penny_wieser@berkeley.edu

See also our GitHub:

[PennyWieser/DiadFit: A python package for fitting Fermi Diads, Ne lines, and other things relating to Raman analyses of CO2 fluids \(github.com\)](#)

Read the docs page:

<https://diadfit.readthedocs.io/>

DiadFit: An Open-Source Python3 Tool for Peak fitting of Raman Data from silicate melts and CO₂ fluids

 Penny E. Wieser ^{*α} and  Charlotte L. DeVitre ^β

^α Earth and Planetary Science, UC Berkeley, CA, USA.

ABSTRACT

We present DiadFit - an open-source Python3 tool for efficient processing of Raman spectroscopy data collected from silicate melts and CO₂ fluids. DiadFit can fit Fermi diads, hot bands, ¹³C peaks, peaks from other gas species (e.g., SO₂, N₂), and Ne emission lines using various background and peak shapes. Thus, it is highly suited for workflows involving melt inclusion vapour bubbles and fluid inclusions (FI). It can also convert between temperature, pressure and density using various CO₂ equations of state (EOS), allowing calculation of FI pressures (and depths in the crust), conversion of homogenization temperatures from microthermometry to CO₂ density, and propagation of uncertainties associated with EOS calculations using Monte Carlo methods. There are also functions to quantify the area ratio of the silicate vs. H₂O region of spectra collected on silicate glasses to determine H₂O contents. Documentation and worked examples are available (<https://bit.ly/DiadFitRTD>, <https://bit.ly/DiadFitYouTube>)

KEYWORDS: Raman spectroscopy; Melt inclusions; Fluid inclusions; Volcanology; Open-source; Python.

1 INTRODUCTION

In recent years, Raman Spectroscopy has been increasingly used by igneous petrologists to perform non-destructive, in-situ measurements of melt and fluid compositions [Steele-Macinnis et al. 2011; Morizet et al. 2013; Hartley et al. 2014; Moore et al. 2015; Schiavi et al. 2018; Giordano et al. 2020; González-García et al. 2020; Schiavi et al. 2020]. Since 2014, there has been a growing body of literature using Raman Spectroscopy to measure the density of CO₂-rich fluids in melt inclusion vapour bubbles to more accurately obtain the total CO₂ content of the melt inclusion, and thus the magma storage depth [Hartley et al. 2014; Moore et al. 2015; Lamadrid et al. 2017; Allison et al. 2021; Wieser et al. 2021; DeVitre et al. 2023b]. Raman spectroscopy also shows enormous potential to quantify the densities of CO₂-rich fluid inclusions [Wang et al. 2011; Kobayashi et al. 2012], allowing rapid and precise estimates of magma storage depths [Dayton et al. 2023].

However, while there have been a large number of studies optimizing calibration and analysis protocols for CO₂-rich fluids by Raman Spectroscopy (e.g., [Lamadrid et al. 2017; Bakker 2021; DeVitre et al. 2021]), there has been comparatively less focus on the software tools and peak fitting routines used to fit Raman spectral data (e.g. [Yuan and Mayanovic 2017]). Many studies use proprietary software supplied as part of the Raman spectrometer for peak fitting (e.g. [Moore et al. 2015]), which affects reproducibility because data is collected (and thus processed) on different Raman instruments (e.g., WITec, HORIBA, Bruker, Renishaw). One popular open-source option is a GUI-based peak fitting program called Fityk ([Wojdyr 2010]). While scripting is possible in this tool, most users fit curves by manually clicking to select peak and background positions (e.g. [DeVitre et al. 2021]). Other studies use OriginLab software which has an annual subscription fee of ~ 200 USD per license per year (e.g., [Hartley et al. 2014]), or have developed their own Matlab/Python codes for specific workflows

and instruments (e.g., [Allison et al. 2021; Wieser et al. 2021]). We do not believe any of the existing data processing methods have been fully optimized for the specific Raman spectroscopy workflows becoming widespread in volcanology, nor do they consider uncertainty associated with peak fitting, instrument drift correction and instrument calibration. There are also no widely-available scripting tools for common calculations associated with fluid inclusion data, such as calculating CO₂ densities from microthermometry data, and converting CO₂ densities from fluid inclusions into pressure and depths using the CO₂ equation of state.

The aim of DiadFit is to provide an open-source, reproducible, easy-to-use, and efficient tool for volcanologists with a wide range of coding experience to fill this gap (Fig. 1). The shapes and locations of the Fermi diad and Ne lines are well defined, and spectra collected on any given Raman instrument have similar features. This means there is enormous potential for automation. In addition to reducing time spent data processing, this will also result in more consistent fitting between different groups, increasing reproducibility. DiadFit is designed so that generic peak fit parameters are tweaked for a specific analytical set up. Using these tweaked parameters, hundreds of spectra can be fitted automatically within minutes, eliminating tedious (and subjective) workflows requiring lots of clicking. Additionally, to align with FAIR principles (Findable, Accessible, interoperable, reproducible), users could publish a supporting folder containing their spectra, relevant metadata, and Jupyter notebooks showing exactly how spectra were fitted (e.g. [Dayton et al. 2023]). DiadFit also outputs the uncertainty associated with each peak fit, which allows for a deeper appreciation of the uncertainty associated with different instrument hardware and acquisition conditions (and a way to quantify improvements).

To demonstrate the time-saving nature of DiadFit, we assess the time taken to fit Neon lines and CO₂ acquisitions collected over a 24 hour period during instrument calibration by [DeVitre et al. 2021]. Fitting these spectra took ~ 8 hrs using

*✉ penny.wieser@gmail.com

Fityk, and ~15 minutes using DiadFit on a typical laptop with 16 GB of RAM and an i7 processor. Given the potential for Raman spectroscopy to provide rapid estimates of magma storage depths from fluid inclusions during volcanic crises (Dayton et al. 2023), it is vital to speed up data processing as much as possible to reap the full benefits of this speedy technique. We anticipate that users who are not familiar with Python will simply use the provided Jupyter Notebooks and narrated YouTube videos, changing simple parameters like the path to their files and peak fit parameters to adjust for the different appearance of spectral peaks on different Raman instruments. More experienced coders can adapt the base functions in DiadFit to create highly customizable workflows to address a number of additional science questions to those targeted here.

2 INSTALLATION

DiadFit can be installed locally on Python versions ≥ 3.7 using either the command prompt (Windows) or the terminal (Mac):

```
pip install DiadFit
```

For Python beginners, we recommend using Jupyter environments (e.g., Jupyter Lab and Jupyter Notebook). In these environments, DiadFit can be installed in a code cell directly:

```
!pip install DiadFit
```

After installation, the user must load DiadFit into their script. Here we load it as `pf`. but users could choose any letters they wish:

```
import DiadFit as pf
```

Any function from DiadFit is then called by typing the chosen abbreviation, followed by a dot, followed by the function name:

```
pf.function_name()
```

Information on what the function does and the required inputs can be accessed using the help function:

```
help(pf.fit_generic_peak)
```

3 UNDERLYING DEPENDENCIES

DiadFit uses peak-fitting functions from the Python package `lmfit` (Newville et al. 2016), which supports iterative fitting of different peak types (e.g., Gaussian, Voigt, Pseudovoigt). The SciPy (Virtanen et al. 2020) `find_peaks` function is used to identify approximate peaks positions and attributes such as height, prominence, and presence/absence of certain peaks. These estimated peak parameters can be used to subdivide spectra into groups with similar characteristics prior to fitting with `lmfit`. Grouping spectra by characteristics, as well as having good estimates of peak position and prominence,

greatly increases computational efficiency during iterative fitting of multiple peaks. Numpy (Harris et al. 2020) is used for all basic math and regression operations, including fitting splines to spectra, and splitting spectra into particular subregions. Pandas (pandas development team 2020) is used for importing data from spreadsheet-type datafiles (.xlsx, .csv), and to output fit parameters in a tabular format. Matplotlib (Hunter 2007) is used for all plots produced by functions. EOS calculations using the Span and Wagner [1996] model are implemented through CoolProp (Bell et al. 2014). This package is not a dependency for all of DiadFit, but if users want to perform calculations using this model, they need to have CoolProp installed (or they will receive an error containing installation instructions). Calculations using this EOS should cite both DiadFit and CoolProp.

4 SUPPORTED FILE TYPES

DiadFit currently supports data input from the following file types. The name given between quotes is the string that should be entered as the `filetype` argument when loading data:

- '**headless_txt**': txt file with no header, with wavenumber in the 1st column and intensity in the 2nd column.
- '**headless_csv**': csv file with no header, with wavenumber in the 1st column and intensity in the 2nd column.
- '**head_csv**': csv file with a header, with wavenumber in the 1st column and intensity in the 2nd column.
- '**Witec_ASCII**': An output from WITec Raman instruments. File starts with '//Exported ASCII-File', then has several lines of metadata, before data is listed under a [Data] heading
- '**HORIBA_txt**': An output from HORIBA Raman instruments that starts with some metadata rows (e.g., #Acq. time), then spectral data is listed under the heading #Acquired
- '**Renishaw_txt**': txt file from a Renishaw instrument where the first header is #Wave, second is #Intensity

If your Raman spectrometer outputs a different filetype, please raise an issue on the DiadFit GitHub providing an example file, or contact the author team by email.

5 PYTHON JARGON

Different calculations in DiadFit are stored within functions. Each of these functions requires users to enter specific input parameters (called arguments), and the function returns various outputs. Five main datatypes are used in DiadFit as inputs or outputs:

- A "**string**" is a piece of text. These are used to tell a function something about your data input, or specify a certain thing you want the function to do. For example,

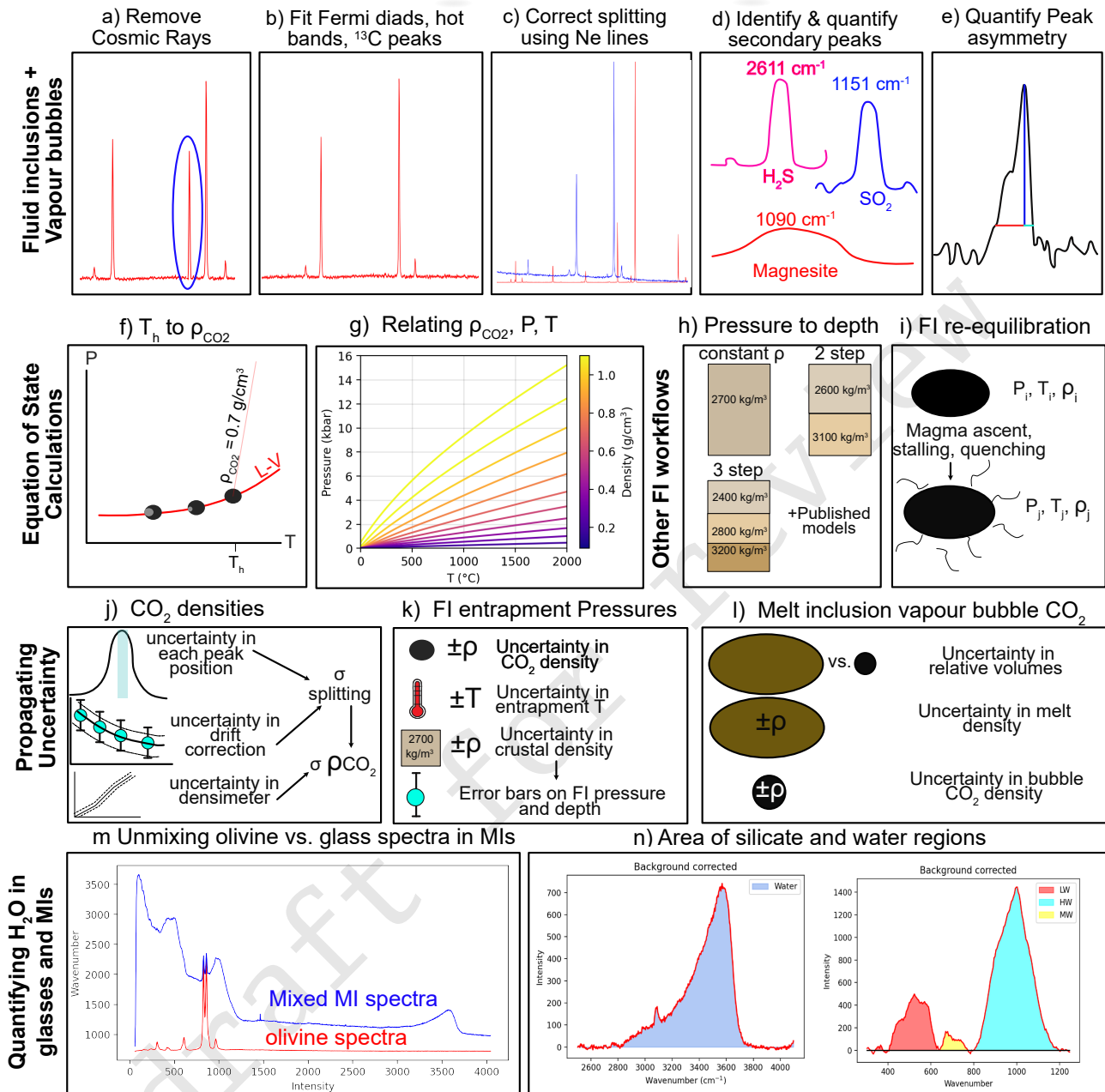


Figure 1: Schematic diagram showing the different workflows that can be performed in DiadFit.

- 165 users must specify their filetype when using functions that load in spectra (e.g., `filetype='headless_txt'`, see Section 4).
- 170 2. A `numpy.array` is a column or array of data without headings. DiadFit uses these to store spectral data after it has been extracted from proprietary instrument files. The wavenumber is stored in the 1st column (index 0 in Python), and the intensity in the 2nd column (index 1 in Python). Numpy is used rather than pandas because it allows for very fast computation.
3. A `pandas.Series` is a column of data with a heading.
4. A `pandas.DataFrame` is a collection of `pandas.Series`, and can be visualized as a single sheet in an excel workbook with labelled columns. In DiadFit, these are used to store peak fitting parameters in columns with column headings (see Step 2, Fig. 5). Information in a given column of the dataframe (called `df`) can be accessed using the column heading: `df['column_heading']`.
5. `dataclasses` are used to provide default configurations to peak finding and fitting functions. These default con-
- 175
- 180

185 configurations can be tweaked as much or as little as required for each specific Raman spectrometer. For example, the default parameters for fitting diad 1 are stored in the dataclass `diad1_fit_config`:

```
diad1_fit_config(model_name='PseudoVoigtModel',
fit_peaks=2, fit_gauss=False,
gauss_amp=1000, diad_sigma=0.2,
diad_sigma_min_allowance=0.2,
diad_sigma_max_allowance=5,
N_poly_bck_diad1=1,
lower_bck_diad1=(1180, 1220),
upper_bck_diad1=(1300, 1350),
diad_prom=100, HB_prom=20,
x_range_baseline=75, y_range_baseline=100,
plot_figure=True, dpi=200,
x_range_residual=20)
```

190 For example, the input argument `model_name='PseudoVoigtModel'` specifies that the diad and hotband peaks should be fitted with a PseudoVoigt function, which is a weighted sum of a Gaussian and Lorentzian distribution that share values for amplitude, center, and full width half maximum. A Voigt distribution function can be used instead simply by stating:

```
pf.diad1_fit_config(model='VoigtModel')
```

195 Any number of these inputs can be tweaked in this manner. For example, if the user only wants 1 peak (e.g., for weak spectra), wants to fit a third degree polynomial to the background, and wants saved figures showing spectra fits to have a dpi of 300:

```
diad1_fit_config(model='VoigtModel',
fit_peaks=1, N_poly_bck_diad1=3, dpi=300)
```

200 Once these dataclasses are tweaked for a a given instrument/set of samples, they can be used to automatically loop through large numbers of spectral files.

6 WORKED EXAMPLES

205 We have produced a number of example Jupyter Notebooks demonstrating specific workflows. These notebooks are available on GitHub and the ReadTheDocs page. We include notebooks showing how to:

1. Fit peaks resulting from CO₂ fluids and correct data for instrument drift using Ne line acquisitions. This example is based on data collected from a high pressure optical cell during Raman densimeter calibration (see DeVitre et al. 2021).
2. In addition to fitting CO₂ peaks, this example shows how to quantify the area of carbonate and SO₂ peaks in spectra collected from natural fluid inclusions hosted in olivine crystals, and calculate molar ratios of different gas species.
3. Fit CO₂ diads and apply a Ne correction model from spectra collected from melt inclusions vapour bubbles using a HORIBA Raman instrument (data from Wieser et al. 2021).

4. Perform calculations using the CO₂ equation of state, including converting homogenization temperatures from microthermometry into CO₂ densities, converting CO₂ densities from Raman or microthermometry into pressures, and then converting these pressures to depths using different crustal density profiles.

5. Propagate uncertainty in microthermometry and Raman-based fluid inclusion barometry into pressure and depth distributions.

6. Model fluid inclusion re-equilibration for different magma ascent, stalling and quenching scenarios following DeVitre and Wieser [2023].

7. Quantify peak asymmetry using the approach of DeVitre et al. [2023a]. This can be very helpful to identify fluid inclusions which contain both liquid and vapour phases at the time of analysis.

8. Quantify H₂O contents in silicate glasses using an approach adapted from Di Genova et al. [2017] and Schiavi et al. [2018].

9. Quantify the ratio of H₂O to silicate glass peaks on Raman acquisitions taken on unexposed olivine-hosted melt inclusions. This can also be used to quantify H₂O contents in exposed silicate glasses (following Di Genova et al. 2017).

10. Propagating Raman and volume uncertainty when determining the contribution from vapour bubble CO₂ to the total CO₂ budget of melt inclusions.

7 FITTING THE CO₂ FERMI DIAD

The Raman spectrum of CO₂ consists of two relatively strong, well-defined peaks collectively called the Fermi Diad. These peaks result from the interaction of a symmetrical stretching mode and an active bending mode in the CO₂ molecule by a process known as Fermi resonance (Lamadrid et al. 2017, Rosso and Bodnar 1995, Fermi 1931). One of the peaks has a wavenumber of ~1280–1290 cm⁻¹ (referred to as diad 1), and the second peak has a wavenumber of ~1386–1390 cm⁻¹ (diad 2). It is well accepted that the distance between diad 1 and diad 2 (commonly referred to as splitting, diad splitting, Fermi Diad separation, or Δ) correlates with the density of the CO₂ fluid. This is because with increasing CO₂ density, diad 1 moves to lower wavenumbers (shift of 6 cm⁻¹ from 0 to 0.8 g/cm³), while the position of diad 2 stays more constant (only varying by ~1–2 cm⁻¹). The exact relationship between diad splitting and CO₂ density, commonly called a 'densimeter', has been shown to vary as a function of instrument hardware and acquisition conditions (DeVitre et al. 2021, Lamadrid et al. 2017).

The Fermi diad is flanked by low intensity hot bands (HBs), which arise from molecules populating the first excited vibron due to their thermal energy at room temperature, which are also perturbed by a Fermi resonance effect. The peak height of the HBs relative to the diads increases with increasing temperature (Rosso and Bodnar 1995), and in general, hotbands

become more pronounced in spectra collected on denser CO₂ fluids. Diad 2 also has a flanking ¹³C peak to its left which becomes more visible as the CO₂ density increases and with increasing proportions of ¹³C relative to ¹²C (Wang and Lu 2022).

In the literature, density estimates from CO₂-rich fluids such as melt inclusion vapour bubbles or fluid inclusions have been obtained by fitting the position of the Fermi diad using various background models combined with Voigt, Pseudovoigt, Gaussian or Lorentzian peaks. These peak fitting routines greatly increases the precision at which the diad splitting can be determined relative to the spectral resolution of the instrument (distance between datapoints). While Raman instruments typically acquire an intensity reading every 0.1–1.5 cm⁻¹, the error of the peak position on a fitted peak can be 10–30× smaller if an appropriate peak profile is fitted (e.g., voigt/pseudovoigt for diads, Yuan and Mayanovic 2017, Fukura et al. 2006; Lin et al. 2007, see also Section 11.1). After the peaks are fit, splitting is calculated and corrected for instrument drift, an instrument-specific densimeter is used to convert corrected splitting into CO₂ density (Lamadrid et al. 2017, DeVitre et al. 2021).

When using DiadFit to peak fit CO₂ spectra, Step 1 is to find all the spectral files you wish to fit (Fig. 3). In step 2-5, spectra are divided into groups, because diads can vary greatly in terms of spectral characteristics, which will require different peak fitting routines to be applied. Spectra collected on CO₂ fluids with low densities, at relatively deep depths, or using low laser power tend to have a weak to non-existent hot bands. Stronger spectra have prominent hot bands and ¹³C peaks which overlap with the tail of the diad peak. In the strongest spectra, the entire region around the diads and hotbands is elevated above the near-linear background seen at greater distance from the diads (Fig. 2). To ensure good fits for all these different spectra types, we suggest users subdivide their spectra into 'Weak', 'Medium' and 'Strong' groups using the steps described below. In Step 2, a single file is selected, and the `identify_diad_peaks` function uses SciPy `find_peaks` to determine approximate peak positions and prominences for the diad, hotbands and ¹³C peaks for each spectra. This function also calculates various additional parameters that can help group spectra (e.g. signal to noise ratios, elevation of the diad-HB region above background). The SciPy `find_peaks` parameters will need tweaking based on instrument hardware and acquisition parameters to ensure the function finds all relevant peaks which are visible (identified peaks are marked with yellow stars in Step 2). After tweaking these SciPy parameters, all spectra files are looped over in Step 3 to determine the approximate peak parameters for each spectra, and these are saved in a dataframe.

In Step 4, these peak parameters are used alongside a filter to remove any cosmic rays present in the spectra. The filtering process calculates the intensity factor F based on the intensity (I) of any given spectral datapoint relative to the intensities of the datapoints to the left and right:

$$F_{i-1} = \frac{I_i - I_{i-1}}{I_{i-1}} \quad (1)$$

$$F_{i+1} = \frac{I_i - I_{i+1}}{I_{i+1}} \quad (2)$$

These two factors are then multiplied together:

$$M_i = F_{i-1} * F_{i+1} \quad (3)$$

If the spectra has a lower intensity to the left of datapoint i, F_{i-1} will be >1. If the spectra also has lower intensity on the right hand side of point i, F_{i+1} will be >1, so M_i will be >>1. High values of M_i for individual pixels are indicative of short, sharp peaks (i.e. most cosmic rays). A datapoint is considered a cosmic ray if M_i exceeds a user determined value (e.g., `dynfact=0.001`). The highest pixel of Diads, HB and ¹³C peaks can also have high M_i values, so any points with an x coordinate equal to an identified peak position (\pm the spectral resolution) are ignored. Users can also enter a custom range, within which no cosmic rays are removed (e.g. the area around the narrow SO₂ peak). If a cosmic ray is identified, the filter is run again, in case the cosmic ray was wider than a single pixel. The pixels identified as cosmic rays are then removed from the spectrum and a new file is saved with the same filename with the addition of the suffix `_CRR_DiadFit`.

After removal of cosmic rays, the `identify_diad_peaks` function is used again to obtain approximate peak parameters without inference from cosmic rays.

In Step 5, the approximate peak parameters from `identify_diad_peaks` are used to divide spectra into groups. A full description of the different parameters used for classification is provided on the ReadTheDocs page, and the most useful parameters will depend greatly on your Raman instrument and samples. In general, spectra should be classified as 'Weak' when none of the peaks are strong enough to interfere with each other (e.g., Fig. 2c). In a set of acquisitions where lots of spectra have no hot band, it would make sense to have the weak group be spectra with only a diad, and no HB. These are best fitted with a single peak (`fit_peaks=1`). If there was then a second group of slightly stronger spectra with a relatively prominent hot band, these could be classified as 'Medium', with 2 peaks fitted around diad 1, and 3 peaks around diad 2. Fitting more peaks helps improve the overall residual because the tails of the diad and hotband peak overlap slightly for higher CO₂ densities, so should be fitted iteratively (Fig. 2f). Spectra with very strong hot bands, clear ¹³C peaks, and greatly elevated troughs between diads and HBs should be placed into the 'Strong' category. These spectra will need to be fitted with two/three peaks, and an additional Gaussian background to recreate the elevation of the spectra in the diad region (`fit_gauss=True`).

In general, the 'Weak' Category is used for spectra that are weak enough there is no need to fit an additional gaussian background or a ¹³C peak. In the gas-cell calibration data of DeVitre et al. [2021] shown in Fig. 3, we use the 'Weak' category for spectra with no ¹³C peak, and no overlap of the tails of HB2 and Diad2 (Fig. 2c). The remaining spectra could be split in two ways. One option is to classify them all as strong (requiring 3 peaks, and a Gaussian background). If a Gaussian background isn't really required (e.g., Fig. 2f), the

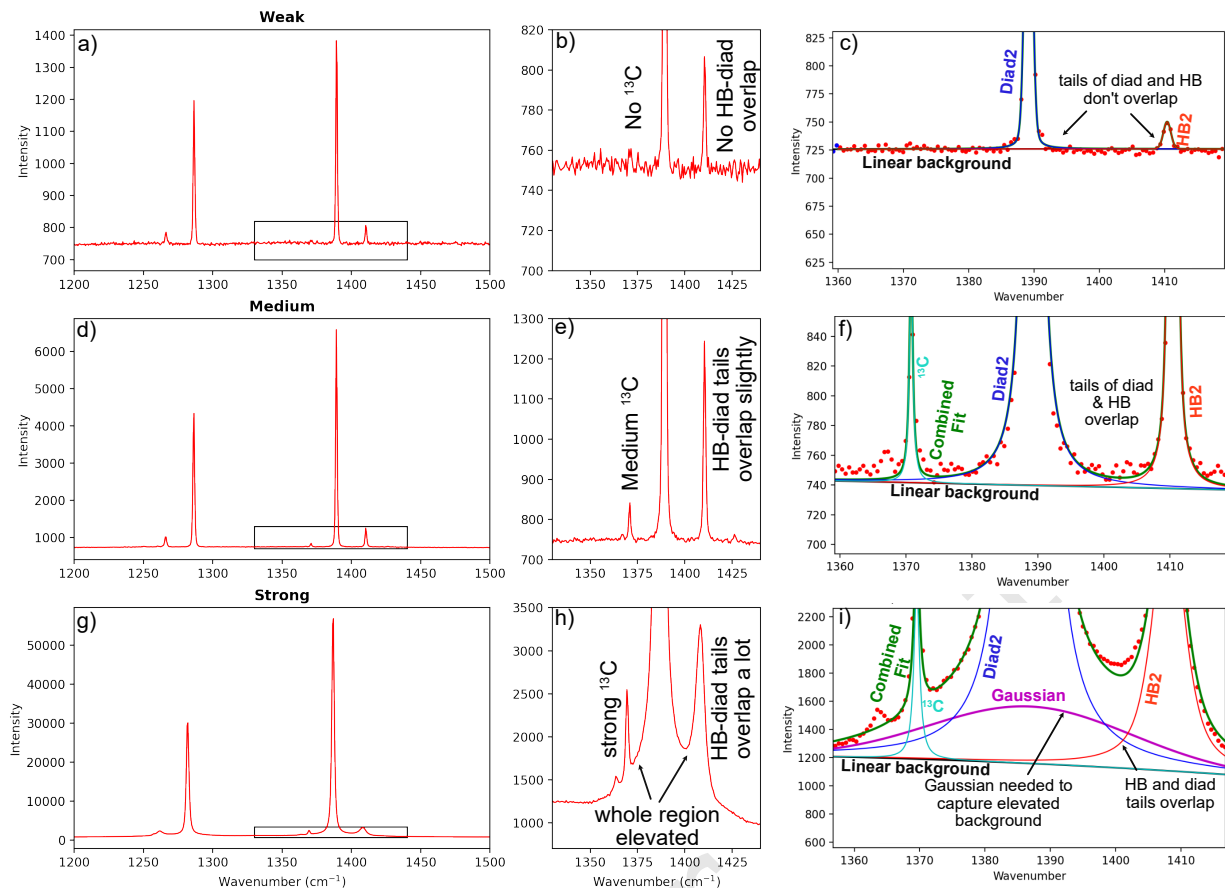


Figure 2: Spectra from DeVitre et al. [2021] with different characteristics can be subdivided into groups for ease of fitting. The weakest spectra (a-c) have no ^{13}C peak, and a small HB, which does not overlap with the diad (c). These could be fitted with 1 or 2 peaks, because the fitting of the HB doesn't influence the fitting of the diad. Slightly stronger spectra (d-f) have a ^{13}C peak, and the tails of the ^{13}C , diad and HB peak all overlap (f). The overlapping tails of these peaks means that 3 peaks need to be fitted iteratively. In the strongest spectra (g-i), the troughs between ^{13}C and the diad and the diad and the HB are greatly elevated above the background. This requires a Gaussian background (purple curve) in addition to the 3 other peaks (red, blue, cyan) to minimise residuals.

code will converge on a Gaussian with a very small amplitude. Thus, the only real advantage of putting those not really
 385 needing Gaussian backgrounds into a 'Medium' Category is that the iterative fitting routine will be a bit faster (favorable when fitting large numbers of spectra).

One file from each group is then used to tweak the fit parameters (Step 6, Fig. 3), which are applied to all spectra in the
 390 group (taking 1-5 s per spectra on a 16 GB laptop). A figure of each fit is produced, and should be visually inspected (Step 8). In Step 9, fit parameters determined through looping over each group are merged together, and combined with relevant meta-
 395 data (e.g. the time stamp needed to apply the Ne correction model). In Step 10, splittings corrected for instrument drift are converted into CO_2 densities using a instrument-specific densimeter. DiadFit incorporates a number of functions to propagate uncertainties (see Section 11.1).

7.1 Fitting peaks to secondary phases

Raman spectra collected from fluid inclusions and melt inclusion vapour bubbles commonly contain peaks arising from

other gaseous species (e.g., SO_2 , N_2) or solid phases on the inclusion wall (e.g., carbonates, sulfates, Schiavi et al. 2020, Frezzotti et al. 2012). It can be helpful to identify which spectra contain such phases, and quantify characteristics of these
 405 peaks (e.g., peak heights, positions, relative peak areas, Burke 2001). As always, step 1 is to obtain all the spectra you wish to fit (Fig. 4). Step 2 uses the function `plot_secondary_peaks` to plot the spectra in a specific wavenumber range from all
 410 selected files. Intensities are normalized based on the range of intensities in the selected wavenumber window, allowing multiple spectra to be stacked and inspected. It is clear from this visualization strategy that files #42 and #33 in Step 2 of
 415 Fig. 4 have prominent carbonate peaks. For any given set of spectra, you can inspect as many regions as you want. For example, the second panel in Step 2 is centered around the SO_2 peak at $\sim 1151\text{ cm}^{-1}$.

As well as plotting spectra to visually identify secondary phases, the function `plot_secondary_peaks` can also identify
 420 peak positions within a user-defined wavenumber range, using either `scipy.find_peaks`, or `peaks` with a specified

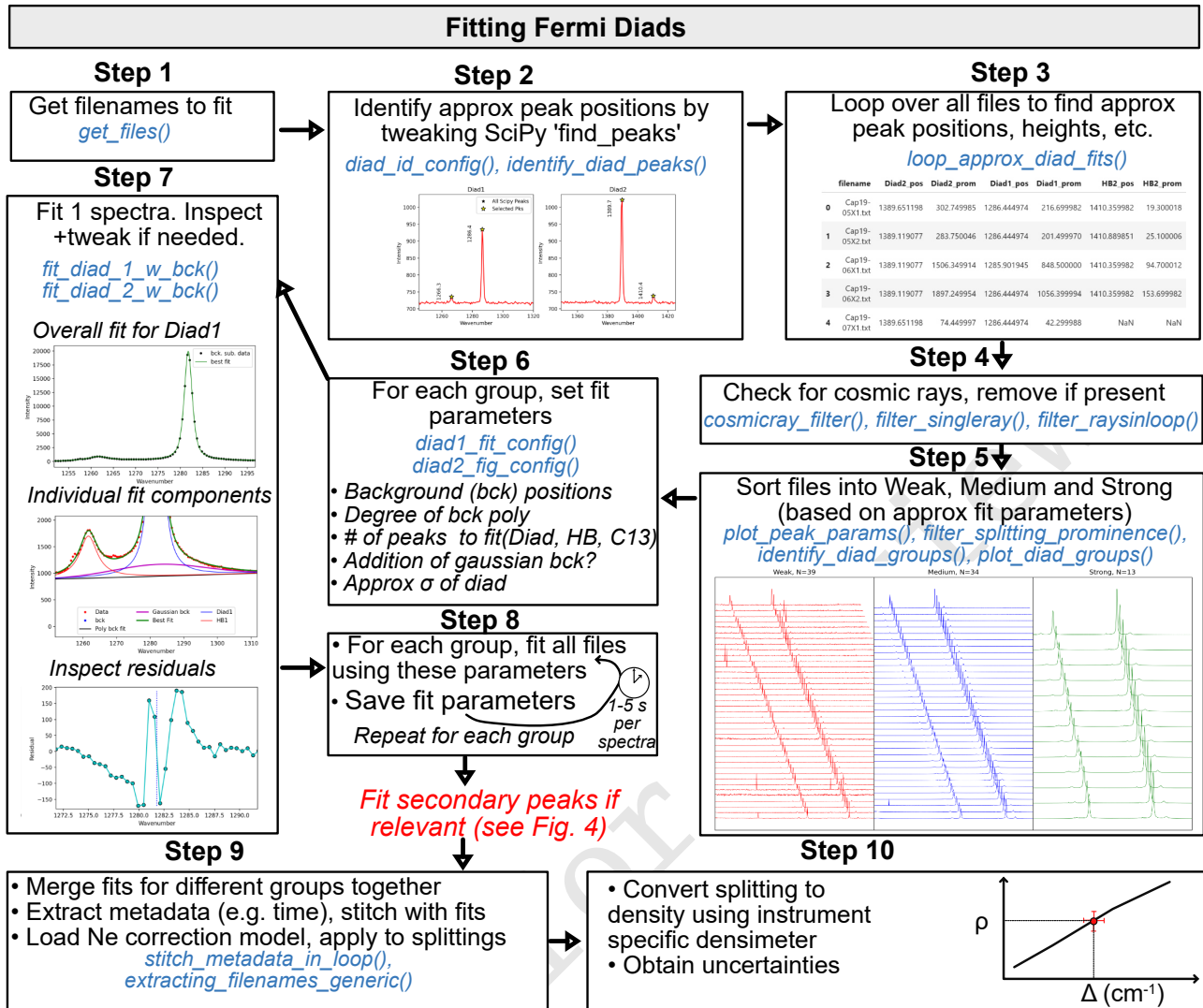


Figure 3: Schematic of workflow used to efficiently fit diad peaks with very different spectral characteristics.

prominence above background noise. Identified peaks will be marked on the returned figure with a yellow star (Fig. 4). The function also returns a dataframe of peak parameters (position, height, prominence) - where no peaks are found, these columns are filled with NaNs. After identifying spectra containing secondary peaks, peak parameters to fit these peaks are tweaked in Step 3 based on a representative spectra. Using the `model_name` parameter, secondary peaks can be fit with Gaussian, PseudoVoigt or Voigt curves, or a cubic spline fit. Tweaked fit parameters are then applied to all files. More than 1 secondary phase can be identified in a given notebook. In Step 5, all identified secondary peaks are merged together with fitting parameters for diad peaks (see Fig. 3).

8 FITTING NE LINES

During any given analytical session, there may be some stretching or contraction of the Raman spectra; these changes are often referred to as 'non-linearity of the Raman shift axis'. For brevity and to draw parallels with various mass spec-

trometry techniques, we term this 'instrument drift'. Commonly, instrument drift within the spectral region containing the Fermi diad is assessed by repeatedly measuring the emission spectrum of Neon (Ne) produced by a lamp every ~ 5 -10 minutes. As well as correcting drift during a given session, Ne can also be used to apply a correction factor between sessions, allowing continued use of a Raman densimeter months to years after it was calibrated. On instruments without a Ne lamp, or with insufficient spectral resolution to quantify the narrow Ne peaks, repeated analyses of standard with known CO_2 density may be used instead.

The Ne emission spectrum has a number of distinctive "lines", several of which lie close to the position of the CO_2 Fermi diad. The wavelength of the different Ne lines in air (λ_1) are converted into Raman shifts (Δ_v) in cm^{-1} using the excitation wavelength of the laser (e.g., $\lambda_0 = 532.05$ nm; Lin et al. 2007):

$$\Delta_v = \frac{10^7}{\lambda_0(\text{nm})} - \frac{10^7}{\lambda_1(\text{nm})} \quad (4)$$

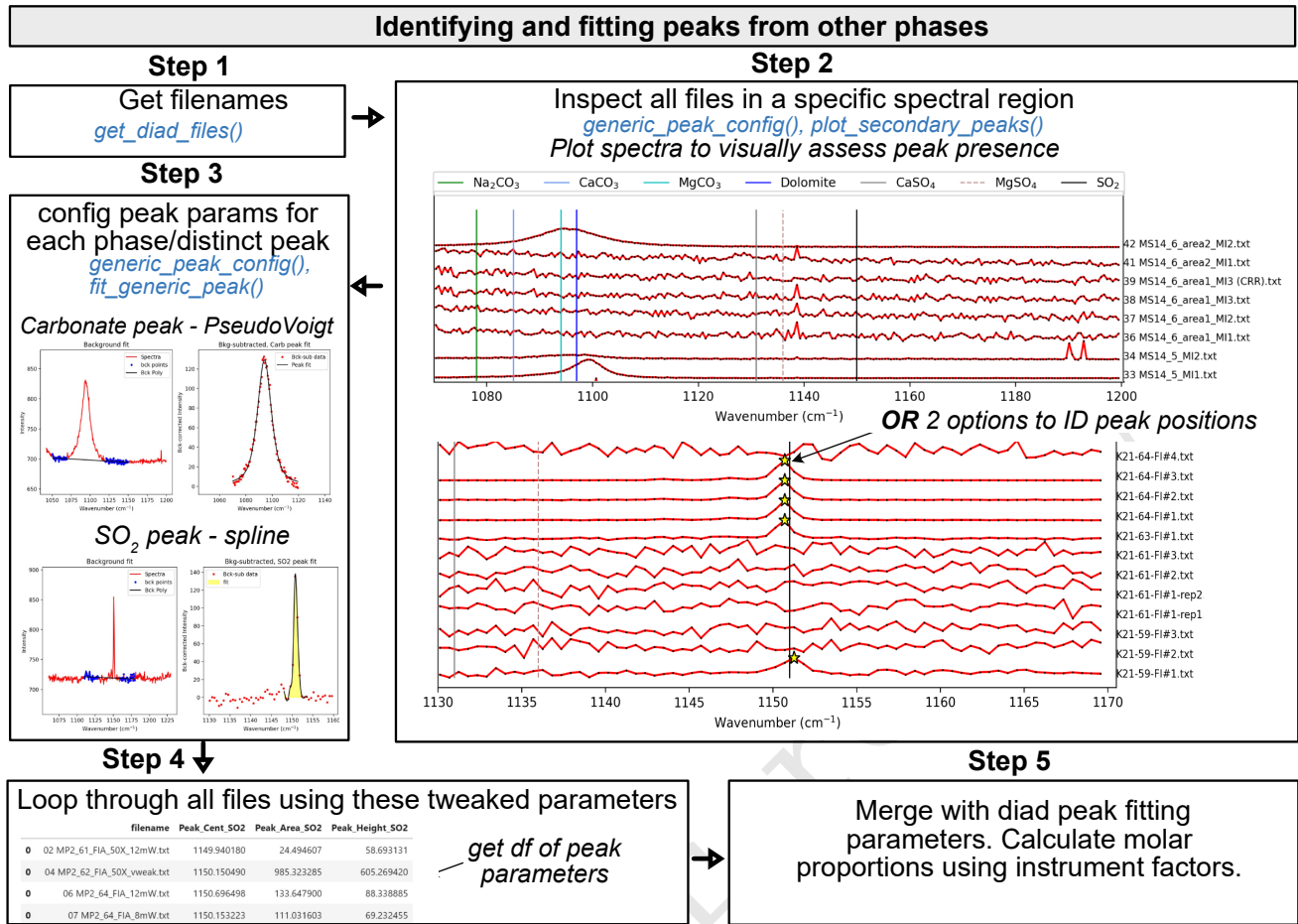


Figure 4: Schematic of workflow used to fit secondary peaks (e.g., carbonate, SO₂). Multiple secondary peaks can be fitted, and all outputs can be merged with diad fit parameters in Step 5.

Traditionally, a given diad acquisition has been corrected for instrument drift and non-linearity by comparing the measured distance between two selected Ne lines ($\Delta_{\text{Ne}}^{\text{Measured}}$) and the theoretical distance between those lines using Equation 4 ($\Delta_{\text{Ne}}^{\text{Theoretical}}$):

$$\text{Correction Factor} = \frac{\Delta_{\text{Ne}}^{\text{Theoretical}}}{\Delta_{\text{Ne}}^{\text{Measured}}} \quad (5)$$

This correction factor is then used to correct the measure diad splitting:

$$\Delta_{\text{CO}_2}^{\text{Corrected}} = \text{Correction Factor} \times \Delta_{\text{CO}_2}^{\text{Measured}} \quad (6)$$

This approach has been termed the 'line segment' technique by Bakker 2021, and a typical workflow of how this method is performed in DiadFit is summarized in Fig. 5. Step 1 identifies all the files which contain Ne lines. Step 2 calculates the theoretical wavenumber of each Ne line using the specific wavelength of your Raman system. You can specify a threshold intensity, and only get lines stronger than that (here, we set the threshold at 2000). This returns a dataframe, with the Raman shift (wavenumber) expected for each Ne line position for your specific wavelength (See Fig. 5 Step 2):

```
df_Ne=pf.calculate_Ne_line_positions(
wavelength=531.885, cut_off_intensity=2000)
```

In Step 3, two Ne lines are selected (1122 cm⁻¹ and 1453⁻¹ in this example), and the theoretical splitting is calculated between the closest lines to those specified wavenumbers. In Step 4, one representative file is selected, and used to tweak peak identification parameters, which are then fed into the Scipy `find_peaks` function to identify the approximate position of each Ne line (and its intensity). Obtaining approximate peak positions and intensities greatly improves the computational efficiency of the fitting process. Default peak identification parameters are stored in the data class `Neon_id_config`, such as the height, prominence, width and threshold to use when identifying peaks using SciPy `find_peaks`. The prominence, defined as the vertical distance above the neighbouring background, is the most important parameter to tweak between different instruments (some instruments have peaks 100s-1000s of counts above background while others are 100,000-1 million counts above background). The function `identify_Ne_lines` uses this tweaked configuration file, and identifies the largest peak within ± 10 datapoints of the Ne line of interest (e.g. for a spectra resolution of 0.4 cm⁻¹ and

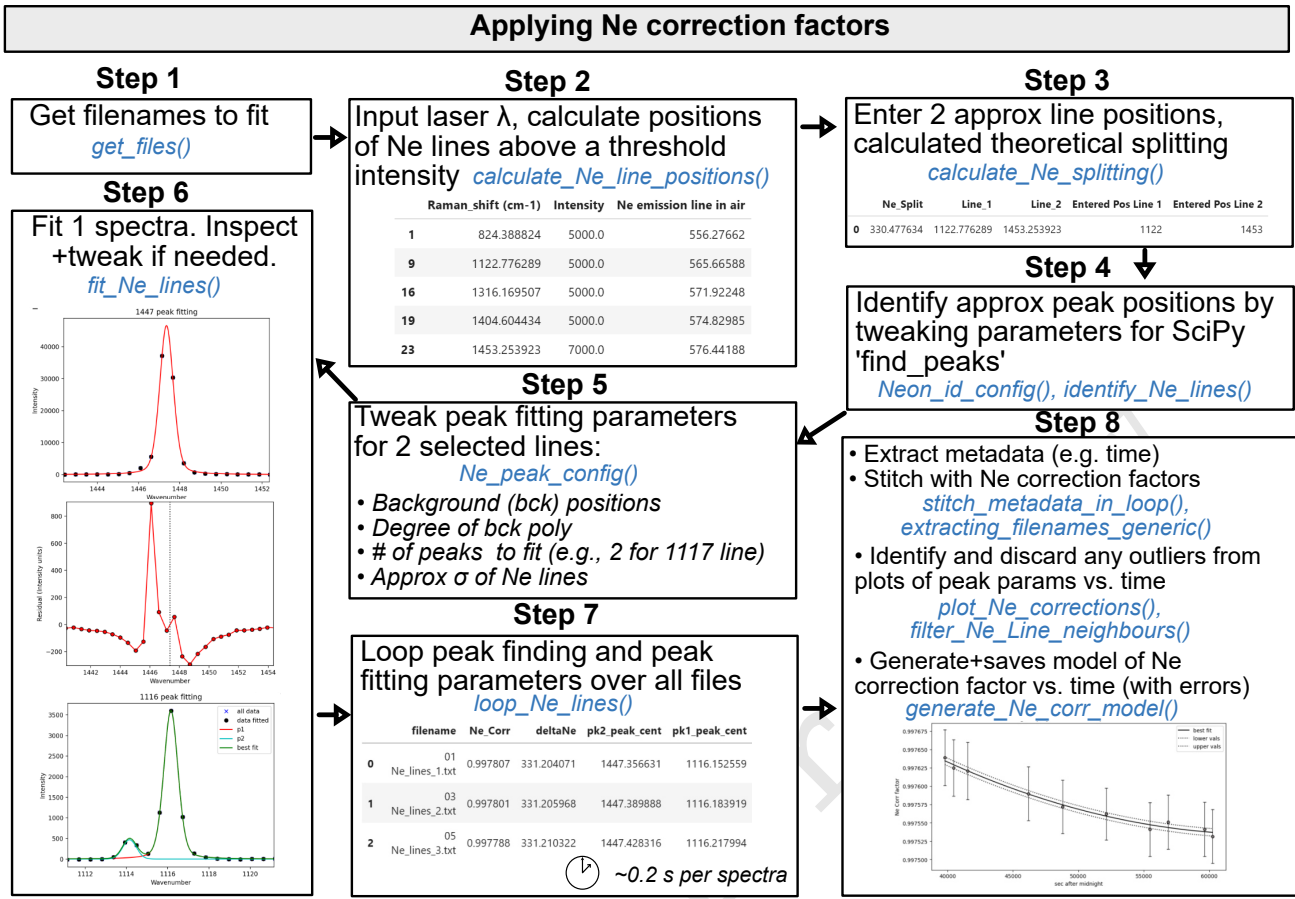


Figure 5: Schematic showing how DiadFit can be used to fit Ne lines, and build a model of correction factor vs. time with full propagation of uncertainty.

495 for line 1122, the spectral region 1118-1126 cm^{-1} would be searched).

After identifying approximate peak positions for each file in Step 4, peak fitting parameters are tweaked in Step 5. The peak fitting function fits a polynomial background to two regions either side of the Ne line, discarding points within this region which are outside of a certain number of standard deviations of the median background position (default 3σ , can be tweaked in `Ne_peak_config`). This background is then subtracted. For most Ne lines, a single PseudoVoigt/Voigt curve can be fitted to background-subtracted data (See $\sim 1453 \text{ cm}^{-1}$ peak in Step 6, Fig. 5). For the line at $\sim 1122 \text{ cm}^{-1}$, two peaks need to be fitted iteratively because of the prominent shoulder to the left of this line (red and cyan curves, combined into the green curve, Fig. 5). Default values specifying how to fit these peaks are stored in a dataclass `Ne_peak_config`, and generally only need tweaking once for each instrument and each selected Ne line. The most important parameters are the positions of the background. These are expressed in terms of distance from the peak center identified above. For example, specifying `lower_bck_pk1=(-40, -25)` positions a background window 40-25 wavenumbers to the left of the peak center. Other important parameters include the degree of polynomial to fit between background points

`N_poly_pk1_baseline=2`, and the approximate sigma of the PseudoVoigt/Voigt curve (`pk1_sigma=0.6, pk2_sigma=0.7`). In Step 6, these tweaked peak fit parameters are used to fit one spectra file with the function `fit_Ne_Lines`. This function returns the peak positions and other fit parameters, as well as graphs showing the overall best fit, the residual of the fit, and the background positions. In addition to plots for visual inspection of residuals, the function also calculates a measure of the residual for each peak:

$$Residual = \frac{\sum \sqrt{(y_{meas} - y_{fitted})^2}}{N_{points}} \quad (7)$$

where y_{meas} is the y-coordinate of the background-subtracted data, y_{fitted} is the y coordinate of the best composite model fit, and N_{points} is the number of discrete points along the x axis used in the fit.

After inspecting these graphs for one Neon acquisition and tweaking any fit parameters as necessary (e.g., background positions, plotting parameters), the `Ne_peak_config` file is updated with the sigma values obtained from this example file (rather than the users guess). The tweaked find peaks and peak fit parameters can then be used to loop through all Ne spectra (Step 7). On a regular laptop (e.g., 16 GB RAM, Intel

i7), it takes approximately 0.2 s to fit each Ne file. There is also an option for the function to save a figure showing the fit for each file in a subfolder it creates within the spectra path. This increases the run time to 1.2 s for each file, but allows users to check the fits, or publish fits as part of a data repository accompanying a paper. After all files are looped through, DiadFit returns a pandas dataframe with the filename, and all the peak fit parameters (including the all important Ne correction factor).

In most published studies, Fermi diad acquisitions have been corrected using the average correction factor of the Ne line acquired before and after a specific sample (although occasionally concurrent acquisitions are used). However, the relatively narrow shape of the Ne peaks means that the error on the peak center of each line, and thus the Ne correction factor, is relatively large (see error bars on Ne correction factor on Fig. 5). Thus, we suggest it may be better to perform a regression of the correction factor as a function of time to average out this random peak fitting noise. On many instruments (e.g., WITec, some HORIBAs), the spectral file doesn't include a time stamp. Sometimes (e.g., WITec), the timestamp is stored in the metadata file, meaning that data and metadata files must be stitched together to obtain the time for each Ne correction factor (see documentation for examples). Alternatively, DiadFit contains functions to extract the time based on the read or edit time stamp on the file. Once a DataFrame is obtained that contains both the Ne correction factor and the time (Step 8), it is useful to inspect changes in Neon correction factors and peak positions with time using built-in visualization functions (e.g., `plot_Ne_corrections`). This allows outliers to be discarded that differ substantially from adjacent acquisitions using the function `filter_Ne_lines_neighbours`. Finally, a polynomial or spline model is used to parameterize the change in Ne correction factor as a function of time (expressed as seconds after midnight, Step 8, Fig. 5), along with the associated confident interval. This model is saved, so that it can be loaded when processing CO₂ spectra from the same session to calculate the correction factor at each point in time (and the associated uncertainty).

It should be noted that Bakker [2021] criticized the 'line segment' technique, because it assumes that the correction factor at any given point between two lines is the same, which is not true if there is any non-linearity in the spectrometer. DiadFit allows users to fit as many different Ne lines as they wish, so more complex Ne correction routines could be utilized (we address differences between drift correction methods in a later contribution).

9 CALCULATIONS INVOLVING THE CO₂ EQUATION OF STATE

An equation of state (EOS) describes the relationship between physical properties of a system such as pressure, temperature and density. EOS calculations are widely used in volcanology - they allow conversion of fluid inclusion densities into pressures, conversion of homogenization temperatures from microthermometry into CO₂ densities, and calculations of densities inside optical cells widely used to calibrate Raman spectrometers. DiadFit currently supports calculations using

the EOS for pure CO₂ using the model of Sterner and Pitzer [1994] (hereafter SP94) and Span and Wagner [1996] (hereafter SW96). While the SP94 EOS is coded directly into DiadFit, we perform calculations using the SW96 EOS through the Python package CoolProp Bell et al. [2014], requiring installation of this package. There are three core functions used to perform EOS calculations in DiadFit:

1. `calculate_rho_for_P_T`: calculates CO₂ density if pressure and temperature are known.
2. `calculate_P_for_rho_T`: calculates pressure if CO₂ density and temperature are known.
3. `calculate_T_for_rho_P`: calculates temperature if pressure and CO₂ density are known.

In systems in equilibrium with mixed fluids (e.g. H₂O in arc magmas), the additional complexities of mixed fluids must be accounted for (see Hansteen and Klügel 2008). Mixed fluid EOS are not currently available in DiadFit, but we hope to add them in future.

9.0.1 Calculating CO₂ density for a given P and T

The function `calculate_P_for_rho_T` can be used to calculate CO₂ density for a specified Pressure (P) and Temperature (T). This calculation is very useful when processing data from Raman calibration apparatus, where T is measured by a thermometer and P is measured with a pressure transducer in the fluid within the optical cell (DeVitre et al. 2021). An entire spreadsheet of pressures and temperatures can be imported and all densities calculated:

```
df=pd.read_excel('Cali_Data.xlsx')
dens_SW96=pf.calculate_rho_for_P_T(
P_kbar=df['P_kbar'], T_K=df['T_K'],
EOS='SW96')
```

9.1 Calculating pressures from CO₂ densities and temperatures

The function `calculate_P_for_rho_T` can be used to calculate pressure for a specified CO₂ density (rho) and temperature (T). This calculation is commonly used to calculate fluid inclusion pressures. This pressure may represent the entrapment pressure under the assumption that the volume and mass of the inclusion is fixed from the point of entrapment to the point at which it is measured in the lab (Roedder 2018), or a re-equilibration pressure if the inclusion underwent prolonged stalling (Hansteen 1991).

To convert a CO₂ density of 0.5 g/cm³ into a pressure at a temperature of 1200 K using the Span and Wagner [1996] EOS (SW96):

```
P_SW96=pf.calculate_P_for_rho_T(
CO2_dens_gcm3=0.5, T_K=1200, EOS='SW96')
```

The Sterner and Pitzer [1994] EOS (SP94) can be used instead simply by changing the EOS argument:

```
P_SP94=pf.calculate_P_for_rho_T(
density_gcm3=0.5, T_K=1200, EOS='SP94')
```

```
CalcDens=pf.calculate_CO2_density_homog_T(
T_h_C=-18, homog_to='L')
```

In addition to single calculations, this function can also be applied to a pandas dataframe with as many rows as the user wants. For example, to load an entire spreadsheet with columns for CO₂ densities and an estimate of entrapment temperatures in °C (as well as an optional column with the sample name):

```
df=pd.read_excel('FI_densities.xlsx')
P_SW96=pf.calculate_P_for_rho_T(
T_K=df['Temp in C']+273.15,
CO2_dens_gcm3=df['Density_g_cm3'],
EOS='SW96', Sample_ID=df['Sample'])
```

This returns a pandas dataframe with calculations done for each input row.

	P_kbar	P_MPa	T_K	CO2_dens_gcm3	Sample_ID
0	0.276826	27.682633	1373.15	0.1	FI1
1	1.559737	155.973743	1473.15	0.4	FI2
2	3.789037	378.903651	1423.15	0.7	FI3
3	10.626112	1062.611174	1473.15	1.1	FI4
4	26.062249	2606.224906	1573.15	1.5	FI5

9.2 Comparing two EOS

DiadFit makes it very simple to compare calculations using the EOSs of [Sterner and Pitzer 1994](#) and [Span and Wagner 1996](#). In Fig. 6, we calculate pressure for 11 discrete densities between 0.1 and 1.1 g/cm³ and temperatures between 34 and 2000 °C (worked example given at ReadTheDocs). These calculations would have been extremely tedious in existing tools, but can be performed in several lines of code in DiadFit (and in seconds of computational time). This figure demonstrates that the EOS are extremely similar at temperatures relevant to basaltic magmas (<2% discrepancies).

9.3 Converting homogenization temperatures to CO2 densities

Microthermometry provides an alternative method to Raman spectroscopy to determine the density of CO₂-rich fluids. A fluid inclusion is cooled down, and then slowly heated up to determine the temperature at which a mix of liquid and vapour transitions to a single homogenous phase (the homogenization temperature). CO₂ densities can be calculated from these homogenization temperatures using the function `calculate_CO2_density_homog_T`. This function uses the homogenization temperature to calculate the pressure based on the position of the L-V phase boundary from [Span and Wagner \[1996\]](#). Once the pressure is constrained, this is used alongside the homogenization temperature to calculate the CO₂ density using the [Span and Wagner \[1996\]](#) EOS (see [Hansteen 1991](#), [Kobayashi et al. 2012](#)). To calculate the CO₂ density of a fluid inclusion which homogenized at -18 ° to a liquid phase:

This returns a DataFrame showing the bulk density, the density of the co-existing liquid and vapour just before homogenization, and the user-inputted parameters.

	Bulk_gcm3	Liq_gcm3	Gas_gcm3	T_h_C	homog_to
0	1.022329	1.022329	0.055156	-18	L

An entire excel sheet of homogenization temperatures and phases can be loaded as a DataFrame. There is also an optional input of entering a sample name for each row (so it is returned in the outputted DataFrame):

```
pf.calculate_CO2_density_homog_T(
T_h_C=df['T_c_Homog'], SampleID=df['Sample'],
homog_to=df['homog_to'])
```

	Bulk_gcm3	Liq_gcm3	Gas_gcm3	T_h_C	homog_to	Sample_ID
0	0.593263	0.593263	0.345003	30	L	FI1
1	0.710471	0.710471	0.242710	25	L	FI2
2	0.773392	0.773392	0.194204	20	L	FI3
3	0.160735	0.821187	0.160735	15	V	FI4
4	0.861096	0.861096	0.135157	10	L	FI5

Uncertainties in homogenization temperature can be propagated to determine errors in density using Monte-Carlo techniques (see example on ReadTheDocs).

10 ADDITIONAL CALCULATIONS RELATING TO FI BAROMETRY

10.1 Converting Pressures into depths

Building on functionality in [Thermobar \(Wieser et al. 2022\)](#), DiadFit can convert pressures to depths using various options (Fig. 1h) implemented in the function `convert_pressure_to_depth`:

- A fixed crustal density (e.g., $\rho=2700$ kg/m³)
- A 2-step crustal density profile (e.g., $\rho=2700$ kg/m³ at <10 km, $\rho=3300$ kg/m³ at >10 km)
- A 3-step crustal density profile
- Pressure-depth models of:
 1. A crustal profile for arc magmas from [Rasmussen et al. \[2022\]](#) ('`rasmussen`').
 2. The combined model of [Mavko and Thompson \[1983\]](#) and [DeBari and Greene \[2011\]](#) as parameterized by [Putirka \[2017\]](#) ('`mavko_debari`') for use in continental arcs.
 3. A crustal profile for Hawaii from [Hill and Zuccal \[1987\]](#) as parameterized by [Putirka \[2017\]](#) ('`hill_zucca`').
 4. A crustal profile for Hawaii from [Ryan \[1988\]](#) parameterized by [Lerner et al. \[2021\]](#) ('`ryan_lerner`').

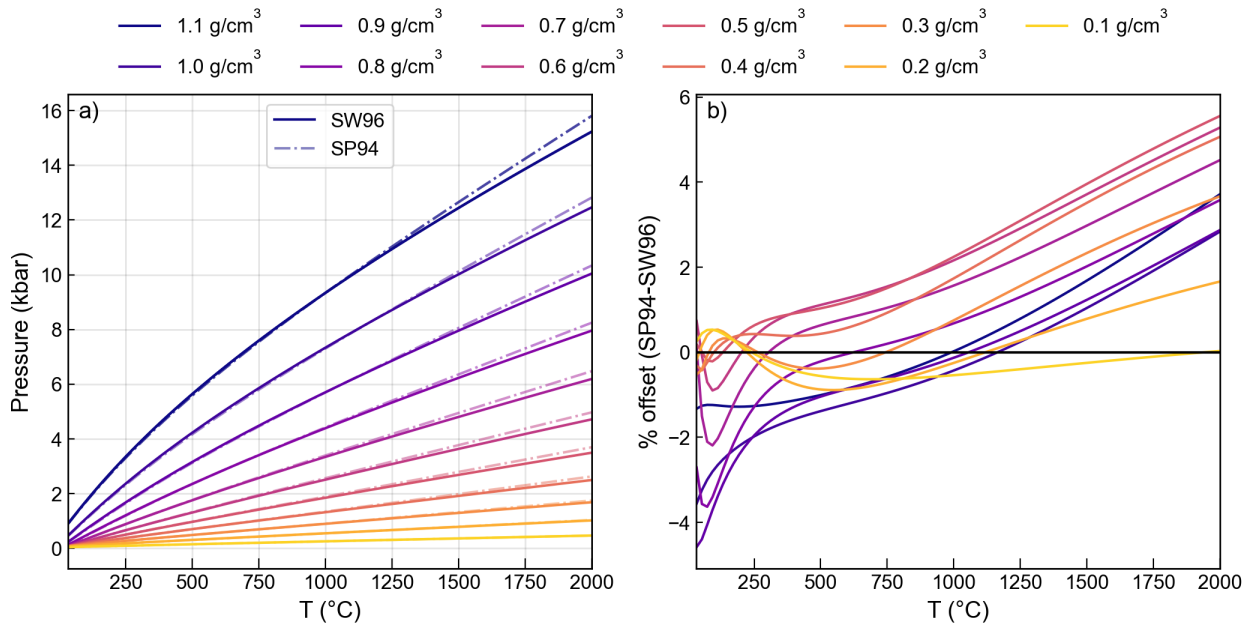


Figure 6: Comparison of the CO₂ EOS of [Sterner and Pitzer \[1994\]](#) and [Span and Wagner \[1996\]](#). The y axis on b) shows the pressure calculated by SP94 minus that from SW96 divided by the average of these two pressures.

We endeavor to add more profiles relevant to different tectonic settings as they become available.

715 For example, to calculate depths using the density profile of [Lerner et al. \[2021\]](#) for the pressures calculated using the SW96 EOS above:

```
D_RL=pf.convert_pressure_to_depth(
P_kbar=P_SW96['P_kbar'], model='ryan_lerner')
```

This returns a pandas Series of depths in km, which could be appended onto the dataframe produced above:

```
P_SW96['Depth_Ryan_Lerner']=D_RL
```

720 This function could be used to investigate a number of different pressure-depth conversions, appending each calculated depth onto a single dataframe for easy comparison.

10.2 Modeling fluid inclusion re-equilibration

725 [DeVitre and Wieser \[2023\]](#) implement a Python3 version of the mechanical re-equilibration model for olivine-hosted fluid inclusions of [Wanamaker and Evans \[1989\]](#) in their package RelaxiFI. We incorporate this package into DiadFit for ease of installation and maintenance, because it uses the underlying EOS and density-depth conversions from DiadFit to track changes in fluid inclusion volume, density, and pressure for different stalling, ascent and quenching paths. Worked examples are available on ReadTheDocs. If this model is used, it should be described as follows 'fluid inclusion re-equilibration was assessed using RelaxiFI [DeVitre and Wieser 2023](#), a Python3 adaptation of the mechanical re-equilibration model of [Wanamaker and Evans \[1989\]](#) implemented through DiadFit v.1.0.74'.

730 For example, the code snippet below shows how to calculate how radius, CO₂ density and internal pressure of a

FI evolve during isothermal ascent (1200 C, 1473.15 K) towards the surface. Specifically, this model considers FI with an initial radius of 1 μm (R) located 100 μm away from a crystal defect (b) ascending from 10 km to the surface in 20 steps (depth_path_ini_fin_step with an ascent rate of 1 m/s (ascent_rate_ms), which is 0.03 MPa/s. Relationships between pressure and density are tracked using the [Span and Wagner \[1996\]](#) EOS (SW96):

```
model=pf.stretch_in_ascent(R_m=10**-6,
b_m=100*10**-6,T_K=1473.15,
depth_path_ini_fin_step=[10,0,20],
ascent_rate_ms=1,EOS='SW96')
```

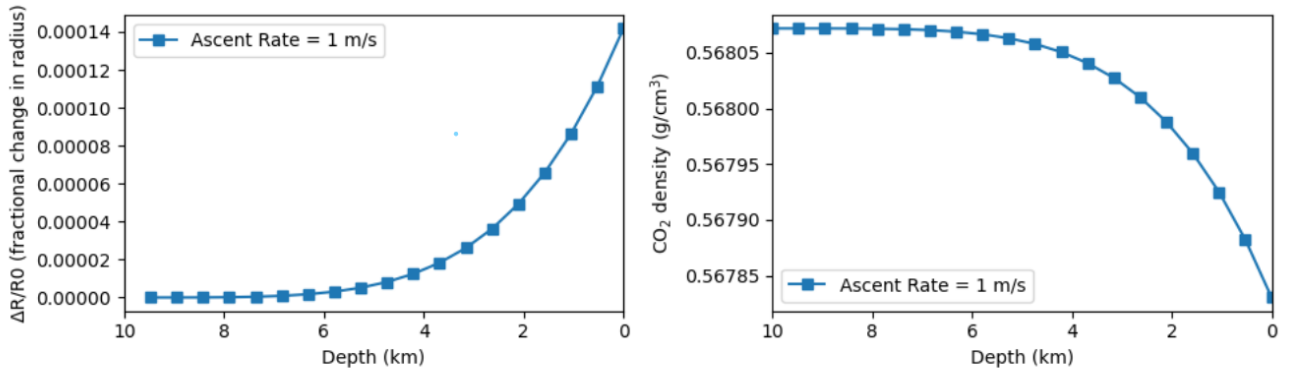
740 This returns a dataframe with columns for time, external pressure change, internal pressure change, stretching rate, FI radius, fractional change in radius, CO₂ density and Depth. Depth can be calculated using the different models available in DiadFit and is an optional argument in the function above configured using `pf.config_crustalmodel()` the default is `pf.config_crustalmodel(crust_dens_kgm3=2750)`, although any of the options in Section 10.1 can be used. The function also returns a figure (See Fig. 7).

11 QUANTIFYING UNCERTAINTY

750 In addition to avoiding tedious busywork, a significant advantage of DiadFit is that it allows rigorous propagation of uncertainty through various volcanological workflows.

11.1 Uncertainty when determining CO₂ density

755 DiadFit provides a framework for propagating the three main sources of analytical uncertainty when quantifying CO₂ density by Raman spectroscopy:



	Time(s)	Step	dt(s)	Pexternal(MPa)	Pinternal(MPa)	dR/dt(m/s)	Fi_radius(μm)	b (distance to xtal rim -μm)	ΔR/R0 (fractional change in radius)	CO2_dens_gcm3	Depth(km)
0	0.000000	0	0.000000	269.775000	269.775000	0.000000e+00	1.000000	100.0	NaN	0.568072	10.000000
1	526.315789	1	526.315789	255.576316	269.774999	1.446726e-18	1.000000	100.0	7.614349e-10	0.568072	9.473684
2	1052.631579	2	526.315789	241.377632	269.774986	1.754262e-17	1.000000	100.0	9.994390e-09	0.568072	8.947368
3	1578.947368	3	526.315789	227.178947	269.774931	7.551312e-17	1.000000	100.0	4.973814e-08	0.568072	8.421053

Figure 7: Screenshot of output from `pf.stretch_in_ascent`, showing the returned figure and the `pandas.DataFrame`

1. Error associated with determining the peak center for each diad (Fig. 8a-b)
2. Error associated with correcting for instrument drift (Fig. 8a-c)
3. Error associated with the densimeter used to convert drift-corrected splitting into CO₂ density (Fig. 8d)

Diadfit obtains the 1σ error associated with each peak center using functionality in `lmfit`. The error associated with the position of each peak center is combined in quadrature to get the error on the peak splitting. The saved Ne line correction model is used to determine the error for the Ne correction factor (Fig. 8c). This error is combined with the splitting error in quadrature to get the uncertainty in the corrected splitting (black crosses, Fig. 8a). To propagate the uncertainty associated with the densimeter, DiadFit uses the regression model through the calibration data. This error is combined with the error on the corrected splitting to yield the overall error in density (σ Density g/cm³, Fig. 8d). Assessing the relative contribution from each source of uncertainty helps optimization of analytical routines (Fig. 8). If the majority of the error is being introduced at the peak fitting stage, it may be that longer acquisitions are required to get stronger signals, or a higher resolution grating is required. Fig. 8a,f shows that a few acquisitions at ~0.18–0.2 g/m³ have far larger peak fitting errors than other acquisitions from the same analytical session. These anomalously large errors would justify inspection of the spectra and fits in more detail, and perhaps re-analysis.

11.2 Uncertainty in fluid inclusion pressures

DiadFit can be used to propagate uncertainty when calculating pressures and depths from fluid inclusions based on

Raman and microthermometry measurements. The function `propagate_FI_uncertainty` allows users to specify uncertainty in CO₂ density, temperature, and crustal density. For each fluid inclusion, the function generates N duplicates of each input variable following the specified error distribution. Pressure (and depths) are calculated for each of these N duplicates, which these are averaged to obtain the mean, median and standard deviation for each FI. Input errors for each variable can be absolute (e.g., ±50 K for temperature) or percentage errors (e.g., ±5%), and can follow a normal or uniform distribution. The function outputs a figure showing the simulation for a single specified fluid inclusion (here, FI1, Fig. 9), in addition to two dataframes. The first dataframe shows the mean, median and standard deviation of calculated pressures and depths for each FI (Fig. 9, Output1). The second dataframe showing the results for all simulations - if N=1000 duplicates and N=10 FIs, the dataframe has 10,000 rows (Fig. 9, Output2).

11.3 Uncertainty in equivalent CO₂ contents of vapour bubbles

The Raman method of reconstructing vapour bubbles present within melt inclusions relies on measuring the CO₂ density, and then converting this into an equivalent amount of CO₂ that would have been dissolved in the glass at the time of melt inclusion entrapment by mass balance:

$$CO_2^{\text{equivalent glass ppm}} = 10^4 \frac{VB \cdot \text{vol \%} \cdot \rho_{CO_2}}{\rho_{\text{melt}}} \quad (8)$$

Thus, the uncertainty in the equivalent CO₂ in the glass depends on the error on the CO₂ density measured by Raman spectroscopy, the uncertainty in the bubble volume, and

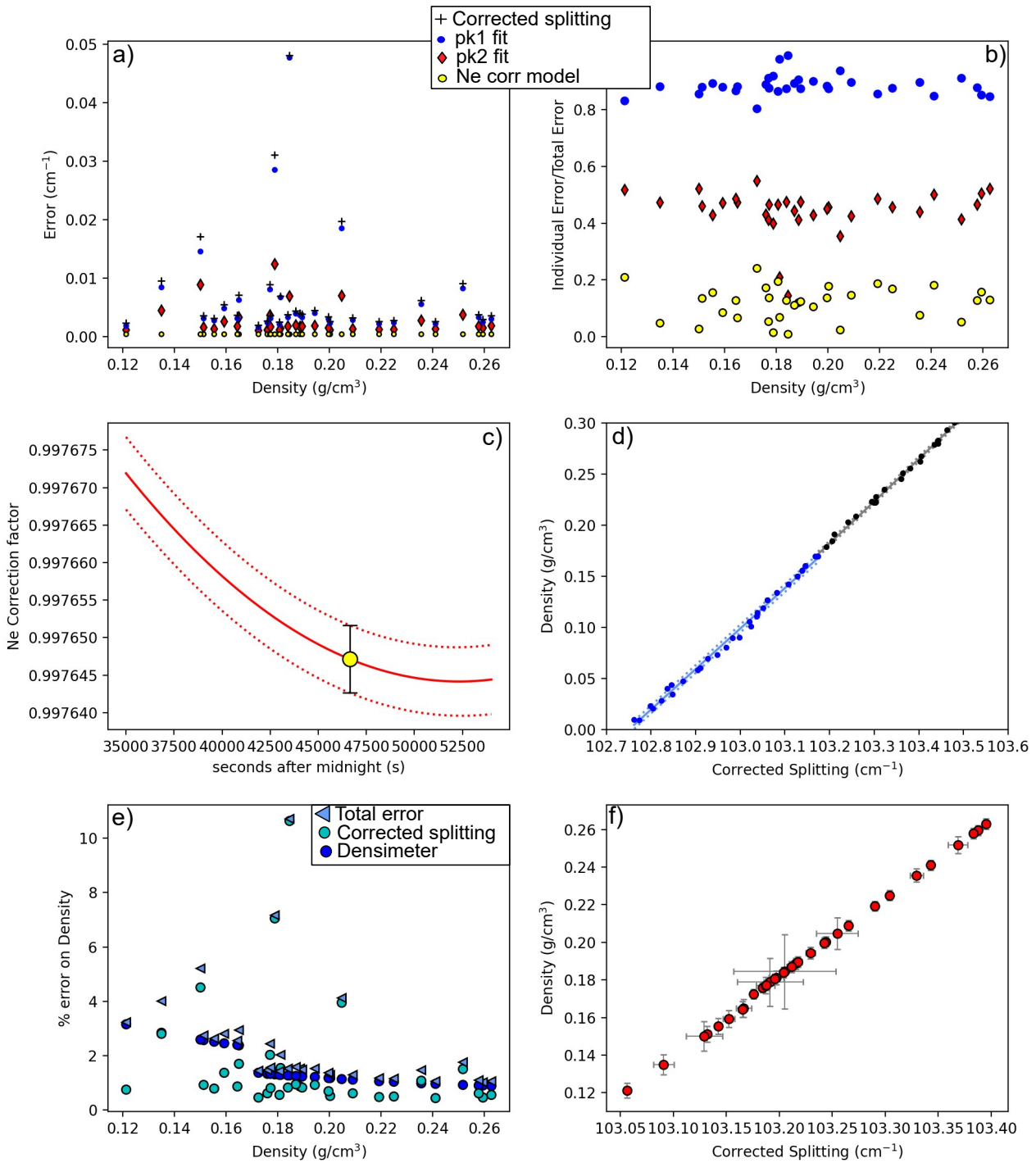


Figure 8: Assessing different sources of analytical error. a) The black cross shows the total error on the corrected splitting from propagating the error in fitting CO_2 peaks and Ne correction model for an instrument with a spectral resolution of 0.56 cm^{-1} . Individual contributions from each peak and the Ne correction model are shown. Note, the total error is smaller than the sum of each error shown, as a result of propagating these errors in quadrature. b) To allow easier comparison of the proportional contribution from each source of error, we also take each individual error and divide by the total error on the corrected splitting. This show that the fitting error on pk1 is the largest source of uncertainty. c) Ne regression model with uncertainty represented by red-dashed lines, along with the uncertainty for a single diad acquisition. d) Error associated with the densimeter shown with dashed lines, with the underlying acquisitions shown as dots. The densimeter is regressed in two parts for low and medium densities (see DeVitre et al. 2021). e) Percentage % error on calculated density, showing the contribution from errors on the corrected splitting (see a) and from the densimeter. f) 1σ errors on density and corrected splitting.

Propagating uncertainty: CO₂ density to pressure and depth

Step 1

Load in CO₂ densities (±Temp and other parameters for plotting)

Sample	Density_g_cm3	T_C	Host_Fo_content
FI1	0.436888	1048.898738	0.897797
FI2	0.417796	1015.924767	0.831850
FI4	0.459045	1041.589916	0.883180
FI5	0.493865	1034.935183	0.869870

Step 2

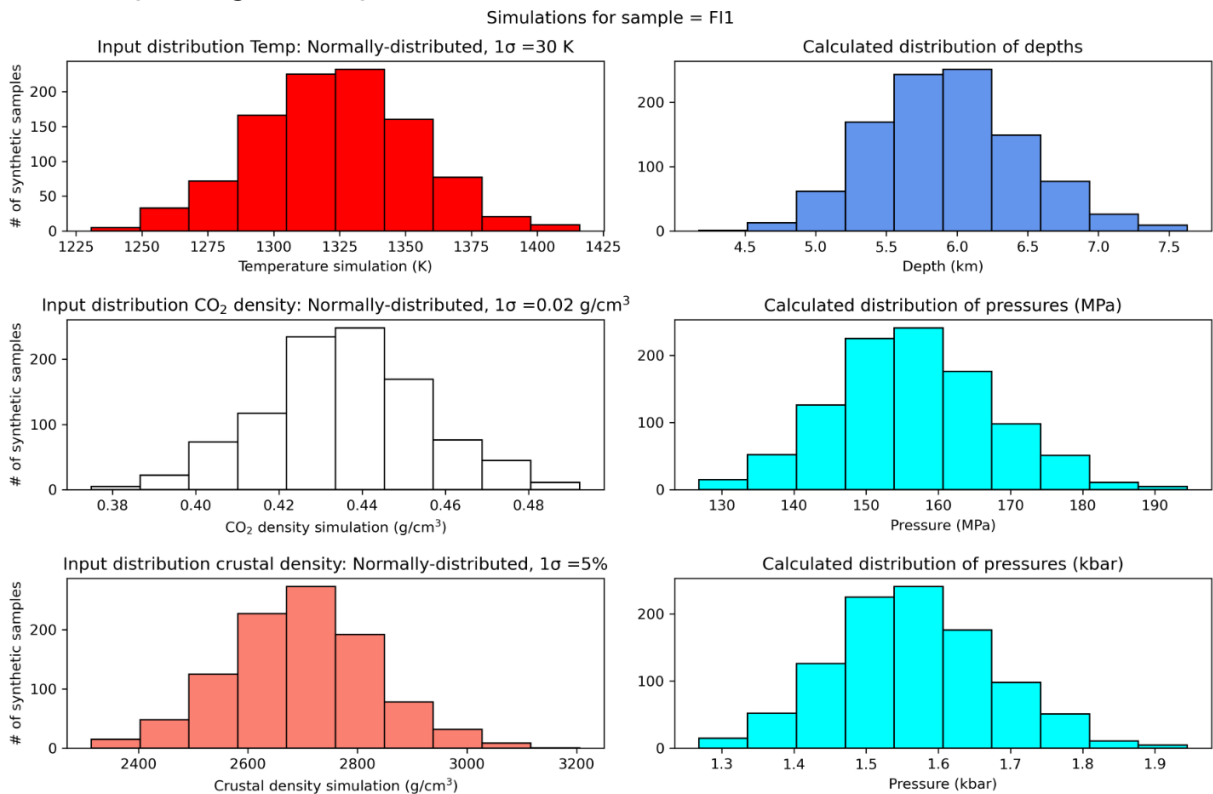
For T, CO₂ and crustal density, select:

- *Magnitude of error, and whether absolute or % (e.g. 5 K, 5%)*
- *Whether error is normally/uniformly distributed*

propagate_FI_uncertainty()

Step 3

Inspect figure outputted from *propagate_FI_uncertainty()* for one FI



Output 1: a dataframe with the average for each FI

Filename	CO ₂ _density_gcm3	SingleFI_D_km	SingleFI_P_kbar	Mean_MC_P_kbar	Med_MC_P_kbar	std_dev_MC_P_kbar	Mean_MC_D_km	Med_MC_D_km	std_dev_MC_D_km	error_T_K
FI1	0.436888	5.920228	1.568091	1.566311	1.561101	0.111547	5.933128	5.923802	0.520378	30
FI2	0.417796	5.382509	1.425665	1.427847	1.420358	0.105647	5.416580	5.374770	0.480109	30
FI4	0.459045	6.337844	1.678705	1.679325	1.670691	0.122355	6.353781	6.306090	0.562820	30

Output 2: A dataframe showing the results for all N simulations for each FI

Filename	Pressure (kbar)	Pressure (MPa)	Depth (km)	input_crust_dens_kgm3	input_T_K	input_CO ₂ _dens_gcm3
FI1	1.745272	174.527165	6.040678	2945.156215	1334.163616	0.465637
FI1	1.481153	148.115300	5.888998	2563.831473	1309.178467	0.423599
FI1	1.477774	147.777421	5.899502	2553.428459	1287.525687	0.428562

Figure 9: Schematic showing the workflow used to propagate uncertainty in CO₂ density, Temperature, and crustal density into error distributions in pressure and depth for each FI.

the uncertainty in calculations of the melt density. As for fluid inclusions, DiadFit contains functionality to propagate these uncertainty using Monte-Carlo methods. The function `propagate_CO2_in_bubble` allows users to specify the magnitude of the error for each parameter, whether the error is a % error or an absolute error, and whether the error is normally or uniformly distributed. This function returns two dataframes - the first with the average and standard deviation for each melt inclusion, and the second showing all simulation outputs. The uncertainty in CO₂ density can be obtained from DiadFit. The uncertainty in melt density can be obtained from [Iacovino and Till \[2019\]](#). Uncertainty in estimating bubble volumes depend greatly on the method used and the geometry of inclusions (e.g., [DeVitre et al. 2023b](#), [Tucker et al. 2019](#)).

12 OTHER USEFUL FUNCTIONS FOR VOLCANOLOGICAL WORKFLOWS

12.1 Quantifying peak asymmetry to identify co-existing liquid and gaseous CO₂

At room temperature (18–22 °C), a CO₂ fluid with a density between ~0.18–0.21 and 0.75–0.79 g/cm³ will consist of an inner shell of CO₂ vapour, and an outer shell of CO₂ liquid (based on the EOS of [Span and Wagner 1996](#)). Using the `calculate_CO2_homog_T` function, we can calculate that at 20 °C the gaseous phase will have a density of 0.194 g/cm³ and the liquid will have a density of 0.773 g/cm³. [DeVitre et al. \[2023a\]](#) show that Raman measurements performed in inclusions with two coexisting phases at room temperature don't always show two distinct peaks for the gaseous and liquid CO₂ phase, but often show a single skewed peak, with contributions from both phases. Quantifying peak asymmetry can help to identify such spectra, which cannot be reliably quantified for CO₂ density.

To assess asymmetry in each spectra, an Nth degree polynomial is fitted between specified baseline positions, and this background is subtracted. A cubic-spline is fitted between the baseline positions. The x and y coordinates of the highest point on this spline fit are identified. The position on each shoulder of the peak with an intensity equal to a certain fraction of the peak height is identified. In Fig. 10, this cut off parameter `int_cut_off` is set at 0.3. The ratio of the x-distance between the peak center and these shoulder points (green and grey lines in Fig. 10) defines the peak asymmetry. After tweaking these parameters for one spectra, the function `loop_diad_skewness` can be used to loop through all files in a specific folder, and stitch the results into a dataframe. Typical skewness parameters have to be identified for each instrument, after which spectra with high skewness can be identified, and reanalysed about the critical temperature where a single peak will be present (see [DeVitre et al. 2023a](#)).

12.2 H₂O fitting

Raman spectroscopy can be used to quantify H₂O within silicate glasses ([Di Genova et al. 2017](#); [Schiavi et al. 2018](#)). There are a number of different methods, with some using the height or intensity of the water Raman band (~3000–3800 cm⁻¹), and others using the ratio of the area under the water re-

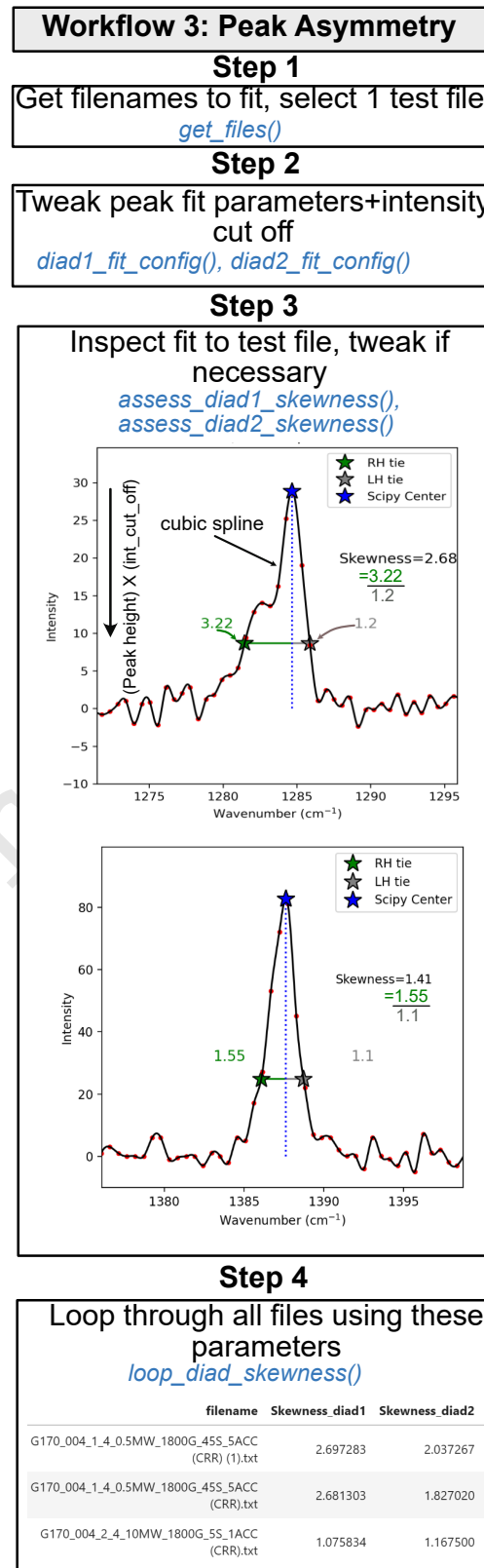


Figure 10: Schematic showing how DiadFit can be used to assess diad asymmetry following the method of [DeVitre et al. \[2023a\]](#).

gion divided by the area under the alumino-silicate band at
~200–1250 cm^{-1} . Specifically, the glass alumino-silicate re-
gion consists of two bands, the low frequency/low wavenum-
ber (LF or LW) band centered on ~550 cm^{-1} , a medium fre-
quency/wavenumber (MF, MW) band centered at ~550 cm^{-1} ,
and a high frequency/wavenumber (HF, HW) band at ~1000
 cm^{-1} (Fig. 11). The exact relationship between peak ar-
eas/ratios/heights and the H_2O content depends on instru-
ment hardware and the glass major element composition, so
standards with known H_2O contents must be used for cali-
bration (Schiavi et al. 2018).

Schiavi et al. [2018] aimed to produce a global calibration,
with less dependence on glass composition. They noted that
the baseline of the silicate region is highly dependent on glass
composition and redox state, and suggested fitting a default
cubic baseline through predefined baseline positions for 4 melt
compositions (basalt, basanite, andesite, rhyolite). They found
that the ratio of the total silicate area (LW+HW±MW) to H_2O
area was reasonably independent of melt composition. How-
ever, González-García et al. [2021] note that the presence of
nanolites with a peak at 670-690 cm^{-1} complicate total sili-
cate area methods, because this nanolite region overlaps with
the LW silicate region used in the 'total area method' of Schi-
avi et al. [2018]. They propose a new protocol using only the
HW area to characterize the silicate portion, rather than the
the overall silicate region as in Schiavi et al. [2020]. To al-
low maximum flexibility when using these different methods,
DiadFit quantifies the HF, LF and LW areas and the overall
silicate area (Fig. 11).

When fitting spectra acquired on hydrous glasses in
DiadFit, the first step is to select the files of inter-
est. As for diads and Ne lines, default peak fit pa-
rameters are stored in dataclasses. There are data-
classes for the four suggested background positions of
Schiavi et al. 2018, e.g., `sil_bck_pos_Schiavi_basalt`,
`sil_bck_pos_Schiavi_andesite`. Users can tweak these
background positions for their specific samples if they wish
(e.g. for a basaltic andesite). For example, the lower back-
ground position can be easily changed for basalt from the de-
fault of 300–340 to 320-350 cm^{-1} :

```
pf.sil_bck_pos_Schiavi_basalt(  
lower_range_sil=[320, 350])
```

These dataclasses also store options for baseline fitting. By
default, a polynomial of degree 3 is used. After subtracting
away the background, an N^{th} degree polynomial is fitted to
the silicate and water regions, and the area under each curve is
calculated using the Simpson and the trapezoid method (Tal-
larida and Murray 1987) implemented in SciPy and NumPy
respectively. The function returns these areas, along with the
ratio of the silicate to water areas for each area method (as well
as other useful parameters such as the positions of chosen
baselines, degrees of polynomials etc. for future reference).

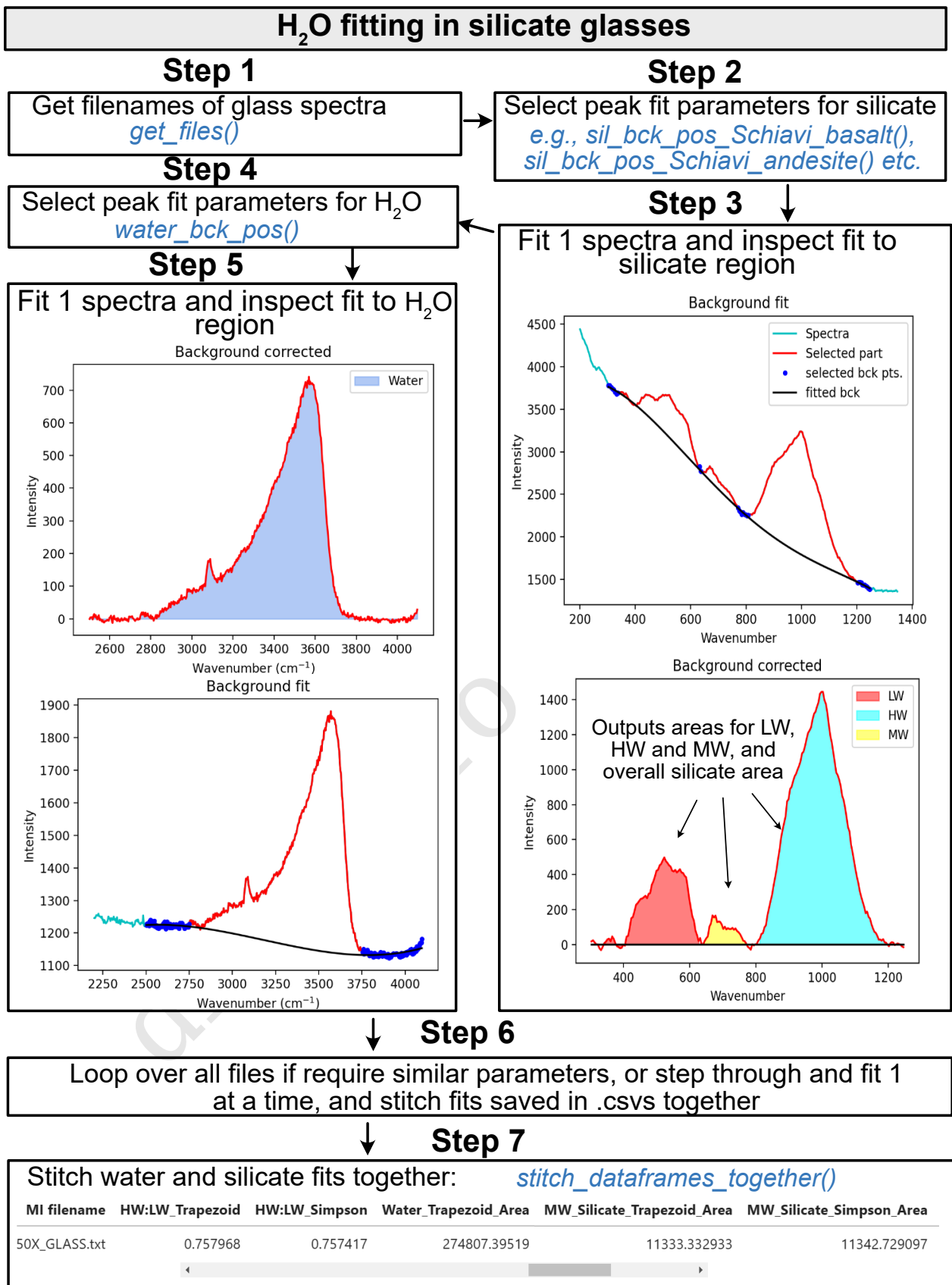


Figure 11: Schematic showing how DiadFit can be used quantify the relative areas of silicate and H₂O peaks in Raman spectra collected from silicate glasses.

12.2.1 H₂O fitting within melt inclusions

A common criticism of the Raman method when quantifying the CO₂ content of vapour bubbles is that it does not account for the sequestration of carbon as solid carbonate phases on the inclusion walls (e.g., Moore et al. 2015). DeVitre et al. [2023b] developed a technique where melt inclusions with carbonate-bearing vapour bubbles are heated to their liquidus temperature using a Linkam TS1400XY stage, causing carbonate to redissolve as CO₂ which can then be measured by Raman spectroscopy. A concern with any heating method when working with melt inclusions is the possibility of diffusive loss of H₂O (Chen et al. 2011; Gaetani et al. 2012). DeVitre et al. [2023b] develop a method to assess H₂O loss by acquiring Raman spectra on unexposed melt inclusion glasses before and after homogenization. We

Quantifying H₂O in spectra acquired from unexposed melt inclusions is more complicated than in exposed glasses, because the Raman signal contains a contribution from the glass and the overlying olivine host. The contribution from the host mineral must be subtracted to obtain an 'unmixed spectra', allowing reliable estimation of the silicate area. Here, we describe the method used for olivine-hosted melt inclusions, although it could be easily adapted for other phases. To reliably unmix the spectra, it is best to acquire a spectra in the melt inclusion at the depth where the H₂O peak is the strongest, and a spectra of the olivine next to the melt inclusions. DiadFit extracts the region of these two spectra between 800-900 cm⁻¹ containing the strong olivine doublet. A cubic spline is fitted to both spectra to smooth out noise. SciPy is used to find the positions of the two strong peaks in the olivine spectra, and the trough position between these peaks. DiadFit then creates N spectra, where the olivine spectra is subtracted from the mixed spectra. For each of these mixed spectra, a linear regression is fit between the two points with the wavenumbers of the identified olivine peaks. The vertical (y) distance is then calculated between this linear regression and the y value at the x-coordinate of the trough (see Step 4, 12). When too little signal from the olivine has been subtracted from the mixed spectra, the trough position will be lower than the linear regression (e.g., Dist=-400 in sketch 1 on Fig. 12, and when too much olivine has been subtracted, the peaks will invert, and the distance will be a positive number. When exactly the right amount of olivine has been subtracted, there will be no clear peaks or troughs, so the distance will be zero. The function fits a curve to this calculated distance vs. the mixing proportion, to determine the best-fit mixing proportion where the distance is zero. The resulting, "unmixed" spectra is taken as the spectra from the melt inclusion itself. Then, the workflow discussed above can be applied to quantify the relative silicate and H₂O area.

13 FUTURE WORK

The open-source nature of DiadFit means that users can customize functions and build their own (either on a local fork, or using a pull request on GitHub). Additionally, we anticipate that we will continue to add workflows as new applications of Raman spectroscopy appear in volcanology. To reflect the evolving nature of this tool, when citing DiadFit, users should

make sure they specify the version they used, obtained using:

```
pf.__version__
```

Care should also be taken to cite the root packages used by DiadFit. E.g., if converting CO₂ densities to pressures using the functions here, we recommend wording similar to this: "CO₂ densities were converted into pressures using DiadFit (Wieser and DeVitre, 2023, v.1.0), using the Equation of State of Span and Wagner [1996] implemented in CoolProp (Bell et al. 2014).

14 CONCLUSIONS

DiadFit will greatly reduce the time required to fit Raman spectral data for volcanological applications, as well as increasing reproducibility between studies. The robust handling of errors and ability to propagate uncertainty using Monte-Carlo methods allows a better grasp of the errors associated with melt and fluid inclusion workflows. Diadfit also simplifies many workflows involving CO₂ equation of state calculations, for many scientific questions. Less time peak fitting = more time for science!

AUTHOR CONTRIBUTIONS

PW conceived the project and lead the code writing (apart from the functions discussed below). CD wrote the cosmic ray removal code, the fluid inclusion relaxation code, and the code to calculate molar proportions from gas peak areas, and came up with the idea for the peak asymmetry method. She performed extensive testing and tweaking of existing functions.

ACKNOWLEDGEMENTS

We are grateful to Felix Boschetty, Lowell Moore, Chelsea Allison, Sarah Hickernell, and Kenneth Befus for providing example Raman file formats from different instruments. We thank Lyndsey Fisher, and Kyle Dayton for providing feedback on the code. PW and CD was supported by UC Berkeley start up funds, the Rose Hills innovator award and NSF grant 2217371

DATA AVAILABILITY

All files are available on GitHub <https://github.com/PennyWieser/DiadFit>. Documentation is available at ReadTheDocs (bit.ly/DiadFitRTD), and YouTube videos explaining various aspects of the tool are available on the DiadFit YouTube channel bit.ly/DiadFitYouTube

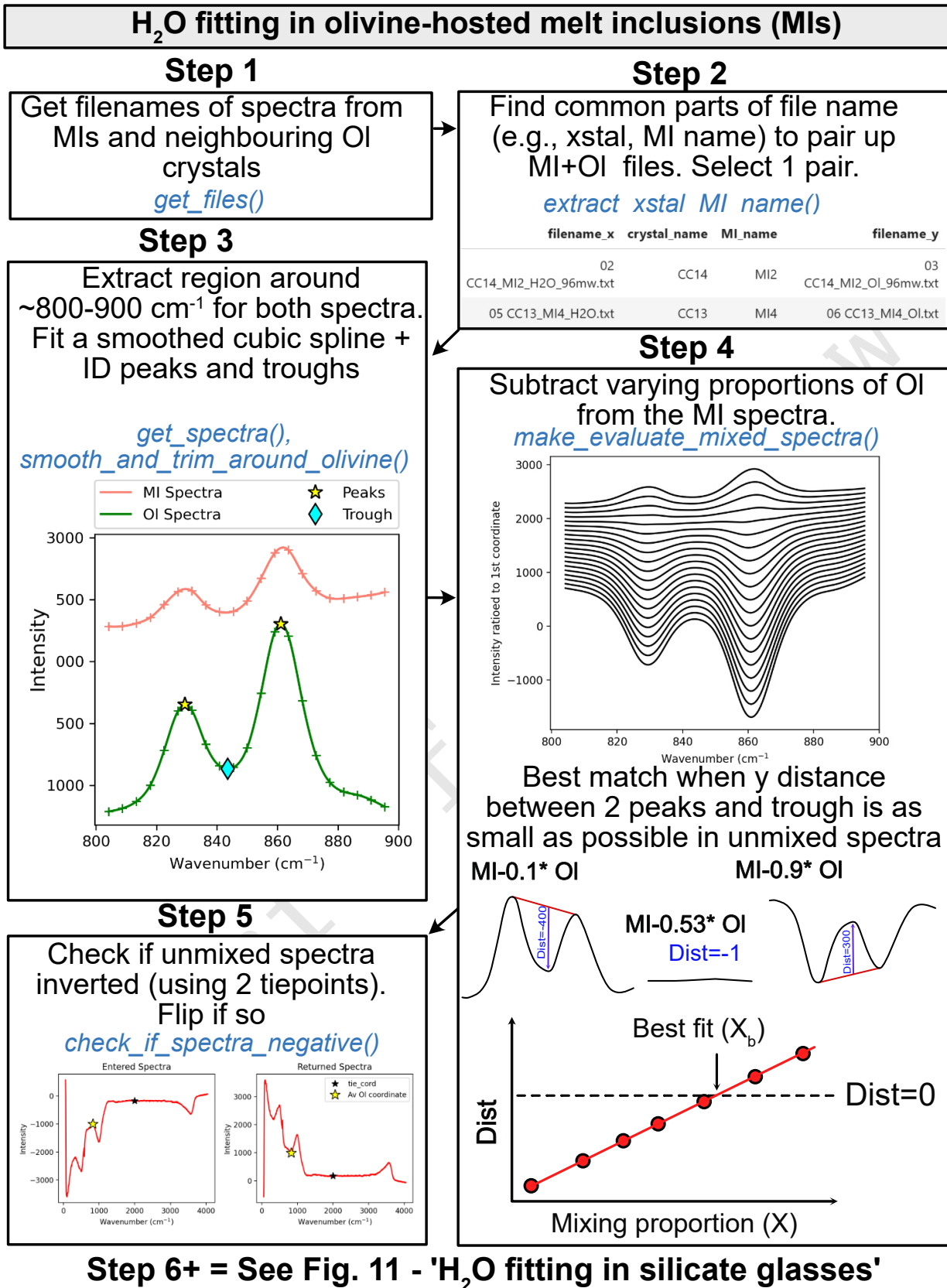


Figure 12: Schematic showing how DiadFit can be used to unmix the contribution of olivine and glass from spectra taken on unexposed melt inclusions. The code could be easily adapted for other silicate phases. There is an option to loop if glass compositions are sufficiently similar. Alternatively, each file can be stepped through manually to tweak positions, and the code saves the output for each file to a .csv, and these are then stitched together after all files are fitted.

COPYRIGHT NOTICE

© The Author(s) 2023. This article is distributed under the terms of the [Creative Commons Attribution 4.0 International License](https://creativecommons.org/licenses/by/4.0/), which permits unrestricted use, distribution, and reproduction in any medium, provided you give appropriate credit to the original author(s) and the source, provide a link to the Creative Commons license, and indicate if changes were made.

REFERENCES

- Allison, C. M., K. Roggensack, and A. B. Clarke (2021). “Highly explosive basaltic eruptions driven by CO₂ exsolution”. *Nature communications* 12(1), pages 1–10. DOI: <https://doi.org/10.1038/s41467-020-20354-2>.
- Bakker, R. J. (2021). “The perfection of Raman spectroscopic gas densimeters”. *Journal of Raman Spectroscopy* 52(11), pages 1923–1948. DOI: <https://doi.org/10.1002/jrs.6245>.
- Bell, I. H., J. Wronski, S. Quoilin, and V. Lemort (2014). “Pure and pseudo-pure fluid thermophysical property evaluation and the open-source thermophysical property library CoolProp”. *Industrial & engineering chemistry research* 53(6), pages 2498–2508. DOI: <https://doi.org/10.1021/ie4033999>.
- Burke, E. A. (2001). “Raman microspectrometry of fluid inclusions”. *Lithos* 55(1–4), pages 139–158. DOI: [https://doi.org/10.1016/S0024-4937\(00\)00043-8](https://doi.org/10.1016/S0024-4937(00)00043-8).
- Chen, Y., A. Provost, P. Schiano, and N. Cluzel (2011). “The rate of water loss from olivine-hosted melt inclusions”. *Contributions to Mineralogy and Petrology* 162, pages 625–636. DOI: <https://doi.org/10.1007/s00410-011-0616-5>.
- Dayton, K., E. Gazel, P. Wieser, V. R. Troll, J. C. Carracedo, H. La Madrid, D. C. Roman, J. Ward, M. Aulinas, H. Geiger, et al. (2023). “Deep magma storage during the 2021 La Palma eruption”. *Science Advances* 9(6), eade7641. DOI: [10.1126/sciadv.ade7641](https://doi.org/10.1126/sciadv.ade7641).
- DeBari, S. M. and A. R. Greene (2011). “Vertical stratification of composition, density, and inferred magmatic processes in exposed arc crustal sections”. In: *Arc-continent collision*. Springer, pages 121–144. DOI: https://doi.org/10.1007/978-3-540-88558-0_5.
- DeVitre, C. L., C. M. Allison, and E. Gazel (2021). “A high-precision CO₂ densimeter for Raman spectroscopy using a Fluid Density Calibration Apparatus”. *Chemical Geology* 584, page 120522. DOI: <https://doi.org/10.1016/j.chemgeo.2021.120522>.
- DeVitre, C. L., K. Dayton, E. Gazel, A. Pamukçu, G. Gaetani, and P. E. Wieser (2023a). “Laser heating effect on Raman analysis of CO₂ co-existing as liquid and vapor in olivine-hosted melt inclusion bubbles”. *Volcanica* 6(2), pages 201–219. DOI: <https://doi.org/10.30909/vol.06.02.201219>.
- DeVitre, C. L., E. Gazel, R. S. Ramalho, S. Venugopal, M. Steele-MacInnis, J. Hua, C. M. Allison, L. R. Moore, J. C. Carracedo, and B. Monteleone (2023b). “Oceanic intraplate explosive eruptions fed directly from the mantle”. *Proceedings of the National Academy of Sciences* 120(33), e2302093120. DOI: <https://doi.org/10.1073/pnas.2302093120>.
- DeVitre, C. L. and P. Wieser (2023). “Reliability of Raman analyses of CO₂-rich fluid inclusions as a rapid barometer at Kīlauea”. DOI: <https://doi.org/10.31223/X5XD4F>.
- Di Genova, D., S. Sicola, C. Romano, A. Vona, S. Fanara, and L. Spina (2017). “Effect of iron and nanolites on Raman spectra of volcanic glasses: A reassessment of existing strategies to estimate the water content”. *Chemical Geology* 475, pages 76–86. DOI: <https://doi.org/10.1016/j.chemgeo.2017.10.035>.
- Fermi, E. (1931). “Über den Ramaneffekt des Kohlendioxyds”. *Zeitschrift für Physik* 71, pages 250–259.
- Frezzotti, M. L., F. Tecce, and A. Casagli (2012). “Raman spectroscopy for fluid inclusion analysis”. *Journal of Geochemical Exploration* 112, pages 1–20. DOI: <https://doi.org/10.1016/j.gexplo.2011.09.009>.
- Fukura, S., T. Mizukami, S. Odake, and H. Kagi (2006). “Factors determining the stability, resolution, and precision of a conventional Raman spectrometer”. *Applied Spectroscopy* 60(8), pages 946–950. DOI: <https://doi.org/10.1366/000370206778062>.
- Gaetani, G. A., J. A. O’Leary, N. Shimizu, C. E. Bucholz, and M. Newville (2012). “Rapid reequilibration of H₂O and oxygen fugacity in olivine-hosted melt inclusions”. *Geology* 40(10), pages 915–918. DOI: <https://doi.org/10.1130/G32992.1>.
- Giordano, D., J. K. Russell, D. González-García, D. Bersani, D. B. Dingwell, and C. Del Negro (2020). “Raman spectroscopy from laboratory and proximal to remote sensing: a tool for the volcanological sciences”. *Remote Sensing* 12(5), page 805. DOI: <https://doi.org/10.3390/rs12050805>.
- González-García, D., D. Giordano, A. Allabar, F. Andrade, L. Polo, V. d. A. Janasi, A. Lucchetti, K.-U. Hess, C. De Campos, and D. Dingwell (2021). “Retrieving dissolved H₂O content from micro-Raman spectroscopy on nanolitized silicic glasses: application to volcanic products of the Paraná Magmatic Province, Brazil”. *Chemical Geology* 567, page 120058. DOI: <https://doi.org/10.1016/j.chemgeo.2021.120058>.
- González-García, D., D. Giordano, J. K. Russell, and D. B. Dingwell (2020). “A Raman spectroscopic tool to estimate chemical composition of natural volcanic glasses”. *Chemical Geology* 556, page 119819. DOI: <https://doi.org/10.1016/j.chemgeo.2020.119819>.
- Hansteen, T. H. (1991). “Multi-stage evolution of the picritic Maelifell rocks, SW Iceland: constraints from mineralogy and inclusions of glass and fluid in olivine”. *Contributions to Mineralogy and Petrology* 109(2), pages 225–239. DOI: <https://doi.org/10.1007/BF00306481>.
- Hansteen, T. H. and A. Klügel (2008). “Fluid inclusion thermobarometry as a tracer for magmatic processes”. *Reviews in Mineralogy and Geochemistry* 69(1), pages 143–177. DOI: <https://doi.org/10.2138/rmg.2008.69.5>.
- Harris, C. R., K. J. Millman, S. J. van der Walt, R. Gommers, P. Virtanen, D. Cournapeau, E. Wieser, J. Taylor, S. Berg, N. J. Smith, et al. (2020). “Array programming with NumPy”.

- Nature* 585(7825), pages 357–362. DOI: <https://doi.org/10.1038/s41586-020-2649-2>.
- 1140 Hartley, M. E., J. MacLennan, M. Edmonds, and T. Thordarson (2014). “Reconstructing the deep CO₂ degassing behaviour of large basaltic fissure eruptions”. *Earth and Planetary Science Letters* 393, pages 120–131. DOI: <https://doi.org/10.1016/j.epsl.2014.02.031>.
- 1145 Hill, D. P. and J. J. Zuccal (1987). “Geophysical constraints on the structure of Kilauea and Mauna Loa Volcanoes and some implications for seismomagmatic processes”. *US Geological Survey Professional Paper 1350* 2(1350), page 903. DOI: <http://pubsdata.usgs.gov/pubs/pp/1987/1350/chapters.html>.
- 1150 Hunter, J. D. (2007). “Matplotlib: A 2D graphics environment”. *Computing in Science & Engineering* 9(3), pages 90–95. DOI: [10.1109/MCSE.2007.55](https://doi.org/10.1109/MCSE.2007.55).
- 1155 Iacovino, K. and C. B. Till (2019). “DensityX: A program for calculating the densities of magmatic liquids up to 1,627 C and 30 kbar”. *Volcanica* 2(1), pages 1–10. DOI: <https://doi.org/10.30909/vol.02.01.0110>.
- 1160 Kobayashi, T., J. Yamamoto, T. Hirajima, H. Ishibashi, N. Hirano, Y. Lai, V. S. Prikhod'ko, and S. Arai (2012). “Conformity and precision of CO₂ densimetry in CO₂ inclusions: Microthermometry versus Raman microspectroscopic densimetry”. *Journal of Raman Spectroscopy* 43(8), pages 1126–1133. DOI: <https://doi.org/10.1002/jrs.3134>.
- 1165 Lamadrid, H., L. Moore, D. Moncada, J. Rimstidt, R. Burruss, and R. Bodnar (2017). “Reassessment of the Raman CO₂ densimeter”. *Chemical Geology* 450, pages 210–222. DOI: <https://doi.org/10.1016/j.chemgeo.2016.12.034>.
- 1170 Lerner, A. H., P. J. Wallace, T. Shea, A. J. Mourey, P. J. Kelly, P. A. Nadeau, T. Elias, C. Kern, L. E. Clor, C. Gansecki, et al. (2021). “The petrologic and degassing behavior of sulfur and other magmatic volatiles from the 2018 eruption of Kīlauea, Hawai'i: melt concentrations, magma storage depths, and magma recycling”. *Bulletin of Volcanology* 83(6), pages 1–32. DOI: <https://doi.org/10.1007/s00445-021-01459-y>.
- 1175 Lin, F., R. Bodnar, and S. Becker (2007). “Experimental determination of the Raman CH₄ symmetric stretching (ν₁) band position from 1–650 bar and 0.3–22 C: Application to fluid inclusion studies”. *Geochimica et Cosmochimica Acta* 71(15), pages 3746–3756. DOI: <https://doi.org/10.1016/j.gca.2007.05.016>.
- 1180 Mavko, B. B. and G. A. Thompson (1983). “Crustal and upper mantle structure of the northern and central Sierra Nevada”. *Journal of Geophysical Research: Solid Earth* 88(B7), pages 5874–5892. DOI: <https://doi.org/10.1029/JB088iB07p05874>.
- 1185 Moore, L. R., E. Gazel, R. Tuohy, A. S. Lloyd, R. Esposito, M. Steele-MacInnis, E. H. Hauri, P. J. Wallace, T. Plank, and R. J. Bodnar (2015). “Bubbles matter: An assessment of the contribution of vapor bubbles to melt inclusion volatile budgets”. *American Mineralogist* 100(4), pages 806–823. DOI: <https://doi.org/10.2138/am-2015-5036>.
- 1190 Morizet, Y., R. A. Brooker, G. Iacono-Marziano, and B. A. Kjarsgaard (2013). “Quantification of dissolved CO₂ in silicate glasses using micro-Raman spectroscopy”. *American Mineralogist* 98(10), pages 1788–1802. DOI: <https://doi.org/10.2138/am.2013.4516>.
- Newville, M., T. Stensitzki, D. B. Allen, M. Rawlik, A. Ingarciola, and A. Nelson (2016). “LMFIT: Non-linear least-square minimization and curve-fitting for Python”. *Astrophysics Source Code Library*, ascl-1606. DOI: [2016ascl.soft06014N](https://doi.org/10.2138/am.2013.4516).
- 1200 Pandas development team, T. (2020). “pandas-dev/pandas: Pandas”. Version latest. DOI: [10.5281/zenodo.3509134](https://doi.org/10.5281/zenodo.3509134).
- 1205 Putirka, K. D. (2017). “Down the crater: where magmas are stored and why they erupt”. *Elements* 13(1), pages 11–16. DOI: <https://doi.org/10.2113/gselements.13.1.11>.
- Rasmussen, D. J., T. A. Plank, D. C. Roman, and M. M. Zimmer (2022). “Magmatic water content controls the pre-eruptive depth of arc magmas”. *Science* 375(6585), pages 1169–1172. DOI: [10.1126/science.abm5174](https://doi.org/10.1126/science.abm5174).
- 1210 Roedder, E. (2018). “Reviews in mineralogy”. In: *Fluid inclusions*. De Gruyter, pages II–II.
- 1215 Rosso, K. and R. Bodnar (1995). “Microthermometric and Raman spectroscopic detection limits of CO₂ in fluid inclusions and the Raman spectroscopic characterization of CO₂”. *Geochimica et Cosmochimica Acta* 59(19), pages 3961–3975. DOI: [https://doi.org/10.1016/0016-7037\(95\)94441-H](https://doi.org/10.1016/0016-7037(95)94441-H).
- 1220 Ryan, M. P. (1988). “The mechanics and three-dimensional internal structure of active magmatic systems: Kilauea Volcano, Hawaii”. *Journal of Geophysical Research: Solid Earth* 93(B5), pages 4213–4248. DOI: <https://doi.org/10.1029/JB093iB05p04213>.
- 1225 Schiavi, F., N. Bolfan-Casanova, R. Buso, M. Laumonier, D. Laporte, K. Medjoubi, S. Venugopal, A. Gómez-Ulla, N. Cluzel, and M. Hardiagon (2020). “Quantifying magmatic volatiles by Raman microtomography of glass inclusion-hosted bubbles”. *Geochemical Perspectives Letters* 16, pages 17–24. DOI: [10.7185/geochemlet.2038](https://doi.org/10.7185/geochemlet.2038).
- 1230 Schiavi, F., N. Bolfan-Casanova, A. C. Withers, E. Médard, M. Laumonier, D. Laporte, T. Flaherty, and A. Gómez-Ulla (2018). “Water quantification in silicate glasses by Raman spectroscopy: Correcting for the effects of confocality, density and ferric iron”. *Chemical Geology* 483, pages 312–331. DOI: <https://doi.org/10.1016/j.chemgeo.2018.02.003>.
- 1235 Span, R. and W. Wagner (1996). “A new equation of state for carbon dioxide covering the fluid region from the triple-point temperature to 1100 K at pressures up to 800 MPa”. *Journal of physical and chemical reference data* 25(6), pages 1509–1596. DOI: <https://doi.org/10.1063/1.555991>.
- 1240 Steele-Macinnis, M., R. Esposito, and R. J. Bodnar (2011). “Thermodynamic model for the effect of post-entrapment crystallization on the H₂O–CO₂ systematics of vapor-saturated, silicate melt inclusions”. *Journal of Petrology* 52(12), pages 2461–2482. DOI: <https://doi.org/10.1093/petrology/egr052>.
- 1245 Sterner, S. M. and K. S. Pitzer (1994). “An equation of state for carbon dioxide valid from zero to extreme pressures”. *Contributions to Mineralogy and Petrology* 117(4), pages 362–374. DOI: <https://doi.org/10.1007/BF00307271>.
- 1250

- 1255 Tallarida, R. J. and R. B. Murray (1987). "Area under a curve:
trapezoidal and Simpson's rules". In: *Manual of Pharmacologic Calculations*. Springer, pages 77–81.
- 1260 Tucker, J. M., E. H. Hauri, A. J. Pietruszka, M. O. Garcia, J. P. Marske, and F. A. Trusdell (2019). "A high carbon content of the Hawaiian mantle from olivine-hosted melt inclusions". *Geochimica et Cosmochimica Acta* 254, pages 156–172. DOI: <https://doi.org/10.1016/j.gca.2019.04.001>.
- 1265 Virtanen, P., R. Gommers, T. E. Oliphant, M. Haberland, T. Reddy, D. Cournapeau, E. Burovski, P. Peterson, W. Weckesser, J. Bright, S. J. van der Walt, M. Brett, J. Wilson, K. J. Millman, N. Mayorov, A. R. J. Nelson, E. Jones, R. Kern, E. Larson, C. J. Carey, Í. Polat, Y. Feng, E. W. Moore, J. VanderPlas, D. Laxalde, J. Perktold, R. Cimrman, I. Henriksen, E. A. Quintero, C. R. Harris, A. M. Archibald, A. H. Ribeiro, F. Pedregosa, P. van Mulbregt, and SciPy 1.0 Contributors (2020). "SciPy 1.0: Fundamental Algorithms for Scientific Computing in Python". *Nature Methods* 17, pages 261–272. DOI: [10.1038/s41592-019-0686-2](https://doi.org/10.1038/s41592-019-0686-2).
- 1270 Wanamaker, B. J. and B. Evans (1989). "Mechanical re-equilibration of fluid inclusions in San Carlos olivine by power-law creep". *Contributions to Mineralogy and Petrology* 102(1), pages 102–111. DOI: <https://doi.org/10.1007/BF01160194>.
- 1280 Wang, W. and W. Lu (2022). "High-precision carbon isotopic composition estimation for individual CO₂ fluid inclusions through Raman spectroscopy". *Geoscience Frontiers*, page 101528. DOI: [10.1016/j.gsf.2022.101528](https://doi.org/10.1016/j.gsf.2022.101528).
- 1285 Wang, X., I.-M. Chou, W. Hu, R. C. Burruss, Q. Sun, and Y. Song (2011). "Raman spectroscopic measurements of CO₂ density: Experimental calibration with high-pressure optical cell (HPOC) and fused silica capillary capsule (FSCC) with application to fluid inclusion observations". *Geochimica et Cosmochimica Acta* 75(14), pages 4080–4093. DOI: <https://doi.org/10.1016/j.gca.2011.04.028>.
- 1290 Wieser, P., M. Petrelli, J. Lubbers, E. Wieser, S. Ozaydin, A. Kent, and C. Till (2022). "Thermobar: an open-source Python3 tool for thermobarometry and hygrometry". *Volcanica* 5(2), pages 349–384. DOI: <https://doi.org/10.30909/vol.05.02.349384>.
- 1295 Wieser, P. E., H. Lamadrid, J. Maclennan, M. Edmonds, S. Matthews, K. Iacovino, F. E. Jenner, C. Gansecki, F. Trusdell, R. L. Lee, et al. (2021). "Reconstructing magma storage depths for the 2018 Kīlauean eruption from melt inclusion CO₂ contents: the importance of vapor bubbles". *Geochemistry, Geophysics, Geosystems* 22(2), e2020GC009364. DOI: [10.1029/2020GC009364](https://doi.org/10.1029/2020GC009364).
- 1300 Wojdyr, M. (2010). "Fityk: a general-purpose peak fitting program". *Journal of Applied Crystallography* 43(5-1), pages 1126–1128. DOI: <https://doi.org/10.1107/S0021889810030499>.
- 1305 Yuan, X. and R. A. Mayanovic (2017). "An empirical study on Raman peak fitting and its application to Raman quantitative research". *Applied spectroscopy* 71(10), pages 2325–2338. DOI: <https://doi.org/10.1177/0003702817721527>.